Polyamine biosynthesis and eIF5A hypusination are modulated by the DNA tumor virus KSHV and promote KSHV viral infection

Authors:

Guillaume N. Fiches[1], Ayan Biswas[1], Dawei Zhou[1], Weili Kong[2], Maxime Jean[3], Netty G. Santoso[1], Jian Zhu[1,*]

Affiliations:

1. Department of Pathology, Ohio State University College of Medicine, Columbus, Ohio, 43210, United States
2. Gladstone Institute of Virology and Immunology, University of California, San Francisco, California, 94158, United States
3. Department of Neurology, University of Rochester Medical center, Rochester NY 14642, USA

* To whom correspondence should be addressed: Jian Zhu (Jian.Zhu@osumc.edu).

Keywords: Polyamine, KSHV, tumor virus, hypusine, eIF5A, lytic replication, latency, ORF50/RTA, ORF73/LANA, ODC1, spermidine

Abstract

Polyamines are critical metabolites involved in various cellular processes and often dysregulated in cancers. Kaposi's sarcoma associated Herpesvirus (KSHV) is a defined oncogenic virus belonging to the sub-family of human gamma-herpesviruses. KSHV infection leads to the profound alteration of host metabolic landscape to favor the development of KSHV-associated malignancies. In our studies, we identified that polyamine biosynthesis and eIF5A hypusination are dynamically regulated by KSHV infection likely through the modulation of key enzymes of these pathways, such as ODC1, and that in return these metabolic pathways are required for both KSHV lytic switch from latency and *de novo* infection. The further analysis unraveled that translation of critical KSHV latent and lytic proteins (LANA, RTA) depends on eIF5A hypusination. We also demonstrated that KSHV infection can be efficiently and specifically suppressed by using inhibitors targeting either polyamine biosynthesis or eIF5A hypusination. Above all, our results illustrated that the dynamic and profound interaction of a DNA tumor virus (KSHV) with host polyamine biosynthesis and eIF5A hypusination metabolic pathways promote viral propagation and oncogenesis, which serve as new therapeutic targets to treat KSHV-associated malignancies.

39 **Introduction**

40 Polyamines, namely putrescine, spermidine and spermine, are low-molecular weight
41 metabolites that are ubiquitous in eukaryotic life. Present in cells at millimolar concentrations,
42 these polycations effectively binds DNA, RNA, and phospholipids thanks to their positive
43 charge at physiological conditions [1] and, in turn, regulate many cellular processes, such as
44 transcription, translation, cell cycle, chromatin remodeling and autophagy [2-7]. Consequently,
45 their metabolism is tightly regulated by multiple layers of feedback loops and interconversion
46 mechanisms [8, 9]. Ornithine decarboxylase 1 (ODC1) is the rate-limiting enzyme that
47 modulates the initial step of the polyamine biosynthesis pathway by converting ornithine into
48 putrescine. Putrescine is then converted into spermidine by the spermidine synthase (SRM)
49 which is subsequently converted into spermine by the spermine synthase (SMS). In addition,
50 catabolic enzymes, such as spermidine-spermine N1-acetyltransferase (SSAT-1), polyamine
51 oxidase (PAO), and spermine oxidase (SMOX), can acetylate or oxidize polyamines to mediate
52 their export and/or convert back to previous stages.

53 However, the homeostatic balance of polyamines is often disrupted in cancers. Indeed,
54 upregulated metabolism of polyamines has been observed in cancers in order to fulfill the
55 increased needs associated with tumorigenesis and rapid growth of tumor cells (reviewed in [10,
56 11]). For instance, polyamines, particularly spermidine, are required for the hypusination of the
57 eukaryotic initiation factor 5A (eIF5A), which has been found upregulated in multiple types of
58 cancers [12-14]. Hypusination is a unique post-translational modification, only reported to
59 occur on eIF5A so far [15, 16], which enables the selective control of protein translation through
60 a conserved biochemical mechanism targeting "hard-to-translate" region, such as polyproline
61 stretches [17, 18]. Consequently, eIF5A hypusination has emerged as a key regulator of the
62 polyamines' downstream cellular processes, such as autophagy [19, 20].

63 Furthermore, investigation of polyamines' role in regulating viral infections started nearly
64 50 years ago. Earlier reports suggested that polyamines benefit the viral packaging of large
65 DNA viruses, such as herpes simplex virus (HSV-1) [21], Vaccinia virus (VACV) [22], and
66 polioviruses [23]. Only very recently, it has been reported that polyamines are involved in the
67 viral life cycle of RNA viruses to promote transcription, translation, and viral packaging,
68 including Zika and Chikungunya viruses [24], Ebola virus [25, 26], Rift valley fever and
69 LaCrosse viruses [27, 28]. In return, viruses often manipulate the polyamine pathway,
70 illustrated by herpesviruses. Human cytomegalovirus (HCMV) is known to induce the
71 expression of ODC1 [29], while ODC1 inhibition using its inhibitor DFMO limits viral
72 replication of HCMV [30]. HSV-1 upregulates the expression of S-adenosyl methionine
73 decarboxylase (SAMDC) [31], while Epstein-Barr virus (EBV) downregulates SSAT-1 [32].

74 In contrast, there is almost no knowledge regarding to the functional contribution of
75 polyamines to Kaposi's sarcoma associated Herpesvirus (KSHV), a relatively recently
76 discovered herpesvirus. KSHV is a human γ-herpesvirus and the etiological agent leading to
77 Kaposi's sarcoma (KS) [33, 34] and associated with two lymphoproliferative disorders, primary
78 effusion lymphoma (PEL) [35] and Multicentric Castleman Disease (MCD) [36]. KSHV has
79 the capacity to establish a life-long infection in the infected individual and persist primarily in
80 infected B lymphocytes and endothelial cells in a quiescent state. During viral latency, only a
81 limited subset of viral latent genes is expressed. Latent infection of KSHV supports the
82 maintenance of viral episomes, and also modulates host cellular environment, including
83 regulation of metabolic pathways, to promote cell proliferation [37-39]. Latent KSHV can be
84 reactivated, and expression of viral lytic genes is turned on and new virions are produced during
85 viral lytic cycle. Although KSHV remains latent in most infected cells, which plays a major
86 role in viral tumorigenesis, lytic replication of KSHV is critical for viral dissemination and also
87 contributes to tumor progression [40, 41]. Hence, it is critical to understand how latent KSHV

88 shapes the host cellular environment to accommodate and benefit its lytic reactivation. In the
89 present study, we reported that polyamine metabolism and eIF5A hypusination are modulated
90 by KSHV, which in return promotes KSHV viral infection.
91
92 **Results**

93 **KSHV dynamically modulates intracellular polyamines.**

94 We first analyzed the global polyamine level in KSHV latently infected tumor cells and also
95 upon lytic reactivation. The renal carcinoma cell line with epithelial-cell origin, known as SLK,
96 and its counterpart cell line latently infected with KSHV BAC16 strain as well as transduced
97 with doxycycline (Dox) inducible RTA, named iSLK.BAC16 [42], were treated with either
98 Dox to induce KSHV RTA expression and consequently lytic reactivation, or vehicle control
99 to keep KSHV at latency. Intracellular total polyamines were stained by using the
100 PolyamineRED reagent [43] and visualized via confocal microscopy. We observed that the total
101 polyamine level was significantly higher in iSLK.BAC16 vs SLK cells without Dox (latent
102 state) (**Fig 1A,B**). However, intracellular polyamines markedly and specifically decreased
103 during lytic replication in Dox-treated iSLK.BAC16 but remained unchanged in the dox-treated
104 naive SLK cells (**Fig 1A,B**). We further analyzed the free, major polyamine species in these
105 cells via thin-layer chromatography (TLC), including putrescine (put), spermidine (spd), and
106 spermine (spm) (**Fig 1C,D**). Putrescine remained relatively stable in both SLK and
107 iSLK.BAC16 cells treated with vehicle control or Dox (**Fig 1C,D, S1A**). Spermine was slightly
108 increased in iSLK.BAC16 vs SLK cells without Dox, while Dox moderately reduced spermine
109 in iSLK.BAC16 cells (**Fig 1C,D, S1C**). On the contrary, spermidine was significantly
110 decreased in iSLK.BAC16 cells at both -/+ Dox conditions (38.3% and 68.6% reduction
111 respectively) (**Fig 1C,D, S1B**). In addition, we also calculated the relative fraction of polyamine
112 species, which revealed that the proportion of spermidine was the most impacted by KSHV

113 latency and lytic reactivation. Spermidine fraction in iSLK.BAC16 cells was indeed lesser than
114 SLK cells at both -/+ Dox conditions (without Dox: 27.6% *vs* 39.9%; with Dox: 19.1% *vs*
115 39.6%), and Dox particularly led to the further decrease of spermidine fraction in iSLK.BAC16
116 cells but not SLK cells (**Fig 1E**). KSHV latency led to a slight increase of spermine fraction
117 (**Fig 1D,E**). However, spermine fraction decreased due to KSHV lytic induction, while
118 putrescine fraction remained stable (**Fig 1D**) resulting in an increase of the relative portion of
119 putrescine (**Fig 1E**). We also performed the above PolyamineRED staining and TLC assays for
120 a KSHV-positive lymphoma cell line transduced with Dox-inducible RTA, TREx BCBL1-RTA,
121 and a KSHV-negative counterpart, BJAB. Similarly, we noticed that the total polyamine level
122 was significantly higher in TREx BCBL1-RTA vs BJAB cells without Dox and that it markedly
123 decreased during lytic replication in Dox-treated TREx BCBL1-RTA cells but not in Dox-
124 treated naïve BJAB (**Fig S1D,E**). TLC assay also confirmed that spermidine was the most
125 reduced polyamine species in Dox-treated TREx BCBL1-RTA cells (**Figure S1F,G**).

126 Taken together, these results clearly showed that KSHV infection distinctly and
127 dynamically modulates the level of intracellular polyamines at latent and lytic phases. It has
128 been reported that c-Myc is upregulated by LANA during KSHV latency [44], while ODC1 is
129 transcriptionally activated by c-Myc [45, 46]. Indeed, we found that ODC1 is slightly
130 upregulated in iSLK.BAC16 vs SLK cells (**Fig 1F**). In contrast, KSHV lytic induction resulted
131 in the decrease of ODC1 protein in Dox-treated iSLK.BAC16 (**Fig 1G**), likely because c-Myc
132 is silenced due to KSHV lytic reactivation [47, 48]. Consistently, we also observed that ODC1
133 mRNA level also decreased at 3 dpi in primary tonsillar B cells isolated from healthy donors,
134 known to be susceptible to KSHV infection and maintain active lytic replication [49], which
135 were spinoculated with KSHV.BAC16 viruses, followed by RT-qPCR analysis (**Fig 1H**).

136 **Polyamine synthesis enzymes are required for KSHV lytic reactivation.**

137 We sought to further determine the contribution of the polyamine pathway to KSHV
138 infection by investigating several key synthesis enzymes from this pathway (**Fig 2A**). ODC1 is
139 critical to catalyze the initial step of polyamine synthesis by converting ornithine into putrescine.
140 HEK293 cells harboring a recombinant KSHV r219 strain (HEK293.r219) were transiently
141 transfected with siRNAs targeting ODC1 or non-targeting (NT) control, and ODC1 knockdown
142 was verified by qPCR and immunoblotting assays (**Fig 2B,C**). TLC assays showed that ODC1
143 knockdown led to the moderate reduction of putrescine and spermine, by 23% and 16%
144 respectively, and the drastic depletion of spermidine by 85% reduction, averaged from three
145 ODC1 siRNAs **(Figure 2D,E**). KSHV r219 strain carries GFP and RFP fluorescent reporter
146 genes allowing visualization of KSHV latent and lytic infection respectively [50]. KSHV lytic
147 reactivation was induced by treating HEK293.r219 cells with 12-O-Tetradecanoylphorbol 13-
148 acetate and Sodium Butyrate (TPA+NaB). Fluorescence imaging indicated that TPA+NaB-
149 induced RFP expression was significantly reduced due to ODC1 knockdown for all three ODC1
150 siRNAs (**Fig 2F**). qPCR assays consistently showed that ODC1 knockdown by its three siRNAs
151 significantly reduces the TPA+NaB-induced expression of KSHV lytic genes, including
152 ORF50/RTA, K8/K-bZIP, and ORF26 genes, respectively representing immediate early, early
153 and late lytic genes (**Fig 2G**), which is supported by the immunoblotting assays confirming the
154 reduced protein level of KSHV lytic genes, ORF45 and K8.1A/B, in HEK293.r219 cells
155 transfected with ODC1 siRNAs (**Fig 2H**). In addition, ODC1 knockdown even reduced the
156 residual expression of KSHV lytic genes that occurs during spontaneous lytic replication (**Fig**
157 **S2A**). The similar effect of ODC1 knockdown on KSHV lytic reactivation was observed in
158 HEK293.r219 cells, in which KSHV lytic reactivation was alternatively induced by ectopic
159 expression of KSHV ORF50 cDNA (**Fig S2B,C**), as well as in iSLK.BAC16 cells treated with
160 Dox+NaB to induce reactivation of latent KSHV (**Fig S2D,E**) . Taken together, data
161 demonstrated the presence of ODC1 is required for the efficient KSHV lytic reactivation.

162 Using the similar approaches, we also determined the relevance of other polyamine
163 synthesis enzymes to KSHV lytic reactivation. Beside ODC1, agmatinase (AGMAT) can
164 convert agmatine to putrescine as well (**Fig 2A**). Although its importance in the polyamine
165 metabolism was initially described for the lower organisms [51], AGMAT has only been
166 recently studied for mammals [52]. Expression of AGMAT was significantly reduced by its
167 two siRNAs in HEK293.r219 (**Fig 3A**), which caused the reduction of TPA+NaB-induced
168 expression of RFP (**Fig 3B**) and KSHV lytic genes (**Fig 3C**) measured by fluorescence imaging
169 and qPCR assays respectively. Putrescine is the shortest biogenic polyamine and converted to
170 spermidine by the spermidine synthase (SRM), which is subsequently converted to spermine
171 by the spermine synthase (SMS) (**Fig 2A**). Two siRNAs targeting SRM or SMS successfully
172 led to their knockdown (**Fig 3D,E**), which also caused the reduction of TPA+NaB-induced
173 expression of RFP **(Fig 3F)** and KSHV lytic genes **(Fig 3G,H)** measured by fluorescence
174 imaging and qPCR assays respectively. SRM or SMS knockdown also reduced the residual
175 expression of KSHV lytic genes that occurs during spontaneous lytic replication (**Fig S3A,B**).
176 In addition, spermidine-spermine N1-acetyltransferase (SSAT-1) is a key catabolic enzyme in
177 the polyamine pathway that acetylates spermidine and spermine, resulting in either their export
178 out of the cell or their conversion by polyamine oxidase (PAO) to putrescine and spermidine
179 respectively. Ribavirin is a FDA-approved drug that has been recently shown to induce SSAT-
180 1 and thus deplete intracellular polyamines [53]. Our results identified that ribavirin severely
181 impairs the Dox-induced KSHV lytic gene expression (**Fig 3I)** and viral genome amplification
182 **(Fig 3J**) in iSLK.BAC16 cells in a dose-dependent manner which was sufficient to increase
183 SSAT-1 protein level (**Fig S3C**) with limited cytotoxicity (**Fig S3D**) in these cells. Collectively,
184 our investigation of several key polyamine synthesis enzymes undoubtedly verified that
185 polyamine homeostasis is critical to KSHV lytic reactivation.

186 **Inhibition of polyamine synthesis efficiently blocks KSHV lytic reactivation.**

187 Inhibitors have been developed to target specific enzymes or steps of polyamine pathway
188 for treating various diseases, especially cancers. α-difluoromethylornithine (DFMO) is a well-
189 tolerated, potent, and irreversible inhibitor of ODC1. Despite its poor pharmacokinetics, DFMO
190 has significant therapeutic potential as a FDA-approved drug for treating trypanosoma (African
191 sleeping sickness) [54], and it also has shown promising results in the on-going clinical trial for
192 treating high-risk neuroblastoma, a severe form of pediatric tumor [ClinicalTrials.gov Identifier:
193 NCT02679144] [55-57]. In our studies, DFMO was used as a chemical probe to inhibit ODC1
194 function and block downstream polyamine synthesis. Following 24hr treatment with DFMO,
195 HEK293.r219 cells were transfected with an ectopic KSHV ORF50 cDNA to reactivate latent
196 KSHV. DFMO reduced the RFP signal in a dose-dependent manner (**Fig 4A**). The qPCR assays
197 of these cells also showed that DFMO significantly decreases expression of KSHV K8/bZIP
198 early lytic gene and the copy number of KSHV genomes with comparable IC_{50} (drug
199 concentration for 50% of maximal inhibitory effect) of 95.9μM and 103.2μM respectively (**Fig**
200 **4B**). DFMO also decreased the expression of KSHV latent genes (ORF71/v-FLIP, ORF72/v-
201 Cyclin, and ORF73/LANA with IC_{50} = 103.2μM, 115.6μM, 210.8μM respectively) in these
202 cells as well. To confirm that DFMO's anti-KSHV effect is through depletion of polyamines,
203 we also performed the rescue experiments by adding exogenous polyamines in the form of
204 polyamines mixture (PA Supp), spermidine (Spd), or spermine (Spm) to the DFMO-treated
205 (500μM ≈ IC_{90}), ORF50-transfected HEK293.r219 cells (**Fig 4C**), which was able to restore
206 the DMFO-inhibited lytic reactivation of KSHV through measurement of RFP-positive cells as
207 well as expression of KSHV lytic genes (K8, ORF26) but caused no obvious cytotoxicity (**Fig**
208 **S4A**). Likewise, DFMO inhibited the Dox+NaB-induced KSHV reactivation in iSLK.BAC16
209 cells as shown through qPCR analysis of copy number of KSHV genomes and KSHV lytic gene
210 expression and immunoblottings (**Fig 4D,E**). Similar effect of DFMO was also confirmed in
211 Dox-treated TREx BCBL1-RTA cells by immunoblottings of KSHV lytic proteins (**Fig S4B**).

212 Alternatively, we also tested clofazimine (CLF), another FDA-approved drug that has been
213 shown to inhibit ODC1 transcriptional activation [58]. CLF is used for treating drug-resistant
214 tuberculosis [59] and has also demonstrated the potential for treating cancers, such as multiple
215 myeloma [58]. Indeed, CLF treatment led to the reduction of Dox-induced KSHV lytic gene
216 expression in iSLK.BAC16 cells in a dose-dependent manner (**Fig 4F**) without obvious
217 cytotoxicity (**Fig S4C**). Overall, these results clearly demonstrated that polyamine synthesis is
218 required for efficient KSHV lytic reactivation, and that FDA-approved drugs inhibiting the key
219 enzyme ODC1 can be used to block KSHV lytic reactivation and the following viral
220 dissemination.

221 **eIF5A hypusination is regulated by KSHV and required for its lytic reactivation.**

222 Autophagy is a critical downstream cellular process regulated by polyamines, particularly
223 spermidine. Spermidine is a unique substrate of the deoxyhypusine synthase (DHPS) that
224 catalyzes the formation of deoxyhypusinated eIF5A, followed by the deoxyhypusine hydrolase
225 (DOHH) mediated hypusination of eIF5A at K50 [60] (**Fig 5A**). Such post-translational
226 modification is very unique and known to only occur to eIF5A [15, 16]), which has been
227 recently illustrated as critical for autophagy activation [19, 20]. It is also known that KSHV
228 RTA induces autophagy [61] that plays a role in KSHV lytic reactivation, likely through
229 transcriptional regulation of autophagy genes, which has been reported in the case of EBV [62].
230 Thus, we postulated that spermidine-regulated eIF5A hypusination connects the upstream
231 polyamine pathway with the downstream autophagy activation and would be important to
232 KSHV lytic reactivation, which has never been investigated. To confirm this thought, we
233 transfected the siRNAs targeting DHPS or NT control in iSLK.BAC16 cells. DHPS was
234 efficiently knocked down by its two siRNAs (**Fig 5B**), which led to the significant decrease of
235 Dox-induced KSHV lytic gene expression in these cells (**Fig 5C**).

236 Reminiscent of earlier studies showing that DFMO blocks autophagy through affecting
237 spermidine [63, 64], we further confirmed that DFMO indeed concurrently reduces the level of
238 hypusinated eIF5A (hyp-eIF5A) as well as impairs autophagy activation assessed by the protein
239 level of p62/SQSTM1 and LC3-I/II while inhibiting KSHV lytic reactivation (**Fig 5D**).
240 Degradation of p62 indicates the lysosomal degradation of autophagosomes and the completion
241 of autophagy events. Protein level of p62 was rapidly depleted in Dox-treated iSLK.BAC16
242 cells, while DFMO restored p62 in both Dox-treated and un-treated cells. DFMO also led to the
243 accumulation of LC3-II but had no severe impact on LC3I in these cells. We also determined
244 that DFMO blocks upregulation of LC3A and IRGM (immunity-related GTPase family M),
245 another important autophagy related gene [65] often found dysregulated during viral infection
246 [66], due to Dox-induced KSHV reactivation in iSLK.BAC16 cells (**Fig S5A**).

247 As we noticed that KSHV infection modulates intracellular polyamine level, we were
248 curious whether it is the same case for eIF5A hypusination. We noticed that the protein level
249 of hypusinated eIF5A is consistently higher in all three tested KSHV-positive lymphoma cell
250 lines (TREx BCBL1-RTA, BCBL1, BC-3) comparing to KSHV-negative BJAB cells (**Fig 5E**).
251 It is also true for iSLK.BAC16 in comparison to SLK cells (**Fig 5F**). These results suggested
252 that, beyond the elevated polyamines, the hypusinated eIF5A was also increased due to KSHV
253 latent infection. In addition, treatment of TPA+NaB to induce KSHV lytic reactivation also led
254 to the slight increase of hypusinated eIF5A in HEK293.r219 cells (**Fig S5B**), suggesting that
255 KSHV lytic reactivation may further impact eIF5A hypusination. Taken together, our results
256 showed that eIF5A hypusination links polyamine pathway to autophagy activation and plays a
257 central role in dynamic host-KSHV interactions regulating viral infection.

258 **eIF5A hypusination determines the translation efficiency of KSHV proteins.**

259 Hypusinated eIF5A plays a critical role in translation elongation by counteracting ribosome
260 stalling during translation of difficult motifs, such as tri-proline (PPP) motif [67-69]. Schuller
261 and colleagues recently described an extended repertoire of 29 motifs whose translation was
262 dependent on hypusinated eIF5A (**Fig S6A**) [17]. The polyamine-hypusine axis is activated in
263 multiple types of cancers, in which protein translation is hypusine-addicted to support cell
264 growth and metastasis, while inhibitors targeting the polyamine-hypusine axis can be used for
265 anti-cancer therapies [12, 14, 70, 71]. Since we also showed that KSHV infection modulates
266 the polyamines-hypusine axis, we wondered whether eIF5A hypusination determines
267 translation efficiency of KSHV proteins. We initially examined the protein sequence of KSHV
268 ORF50/RTA (YP_001129401.1) for hyp-eIF5A-dependency motifs and identified 8 such
269 motifs previously described by Schuller et al (**Fig 6A**). These sites are conserved across
270 multiple KSHV strains (**Table S1**). We tested the impact of eIF5A hypusination on KSHV
271 ORF50/RTA protein translation by using the DHPS-targeted eIF5A hypusination inhibitor,
272 GC7 (N1-guanyl-1,7-diaminoheptane) [20, 72]. GC7 treatment led to the drastic reduction of
273 Dox-induced KSHV RTA expression in iSLK.BAC16 cells (**Fig 6B**), which correlated with the
274 reduction of hypusinated eIF5A as well as the inhibition of p62 accumulation, while GC7
275 caused neglectable cytotoxicity (**Fig S6B**). To further confirm, we ectopically expressed a
276 cDNA of KSHV ORF50/RTA in SLK cells treated with GC7. Protein level of KSHV RTA was
277 significantly lower due to GC7 treatment (**Fig 6C),** but its mRNA level was even moderately
278 increased by GC7 (**Fig S6C**). On the contrary, we also tested GC7's effect on expression of a
279 GFP protein (CopGFP) that has no such difficult-to-translate motifs, which failed to lower
280 protein level of GFP quantified by GFP-positive cells as well as MFI of GFP fluorescence (**Fig**
281 **S6D,E**). Likewise, GC7 had no effect on EBV BZLF1/Zta protein level, since EBV BZLF1
282 only carries 2 hyp-eIF5A-dependency motifs (**Fig 6D, S6F**). Overall, these data confirmed that
283 hypusinated eIF5A is important and specifically controls KSHV RTA protein translation.

284 In parallel, we also examined the protein sequence of KSHV ORF73/LANA
285 [YP_001129431.1] and identified 19 hyp-eIF5A-dependency motifs (**Fig 6E**), which are mostly
286 conserved across multiple KSHV strains (**Table S2**). We tested the impact of GC7 on KSHV
287 ORF73/LANA expression in KSHV latently infected cells, iSLK.BAC16 (**Fig 6F**) and BCBL1
288 (**Fig 6G**) cells. In both cases, GC7 led to the significant decrease of LANA protein. To further
289 confirm, we ectopically expressed a cDNA of KSHV ORF73/LANA in SLK cells treated with
290 GC7. Protein level of LANA was significantly lower due to GC7 treatment but not its mRNA
291 level (**Fig 6H, S6C**). Therefore, our results showed that eIF5A hypusination is critical to KSHV
292 infection since it determines the translation efficiency of KSHV key lytic and latent proteins
293 (RTA, LANA).

294 **Inhibition of eIF5A hypusination potently restricts KSHV viral infection.**

295 Since we showed that translation of KSHV key lytic and latent proteins (RTA, LANA) is
296 hypusine-addicted and can be efficiently blocked by GC7, we speculated that eIF5A
297 hypusination would be a promising host target for developing anti-KSHV therapies. As a proof
298 of principle, we tested the anti-KSHV potency of GC7 as an eIF5A hypusination inhibitor.
299 Indeed, GC7 treatment suppressed the Dox-induced expression of KSHV lytic genes in a dose-
300 dependent manner with similar IC_{50} = 10.0μM, 10.1μM, 7.5μM for ORF50/RTA, K8, ORF26
301 respectively (**Fig 7A**). It was confirmed by immunoblotting of KSHV ORF45 lytic protein in
302 above cells (**Fig 7B**). Similarly, GC7 also suppressed KSHV lytic reactivation in Dox-treated
303 TREx BCBL1-RTA cells in the dose-dependent manner (**Fig 7C,D**) without obvious
304 cytotoxicity (**Fig S7A**). We also showed that GC7 severely impairs the amplification of KSHV
305 viral genomes in these cells (**Fig 7E**). GC7 demonstrated comparable anti-KSHV effect in
306 HEK293.r219 cells treated with TPA+NaB to induce KSHV reactivation (**Fig 7F, S7B**).
307 However, GC7 treatment failed to inhibit EBV lytic gene expression in Akata/BX cells treated
308 with human IgG to induce EBV reactivation (**Fig S7C**). Overall, these results demonstrated that

309 inhibition of eIF5A hypusination by GC7 potently and specifically restricts KSHV lytic
310 reactivation but not EBV.

311 Furthermore, we determined the effect of GC7 on KSHV *de novo* infection. SLK cells were
312 subjected to brief spin infection with KSHV.BAC16 viruses (MOI = 0.5). Unbound viruses
313 were washed away, and cells were treated with GC7. KSHV infection rate was quantified by
314 measuring the GFP expression from KSHV viral genomes in the infected cells. Fluorescence
315 imaging showed that GC7 significantly reduces GFP expression in KSHV-infected SLK cells
316 at 2 days post of infection (DPIs) in the dose-dependent manner (**Fig 7G,H**). We also performed
317 the similar assays using primary tonsillar B cells, which have been shown susceptibility to
318 KSHV infection and support active lytic replication of KSHV for up to 5 DPIs [49]. Hence,
319 primary tonsillar B cells from healthy donors were isolated and subjected to brief spin infection
320 with KSHV.BAC16 viruses (MOI = 3). Unbound viruses were washed away, and cells were
321 treated with GC7. Expression of KSHV lytic (ORF50/RTA, K8) and latent (ORF73/LANA)
322 genes at 3DPIs were analyzed by qPCR assays, which clearly showed that GC7 significantly
323 reduces KSHV viral gene expression in tonsillar B cells from four donors (**Fig 7I**) without any
324 cytotoxicity (**Fig 7J**). These results suggested that eIF5A hypusination also participates in the
325 early steps of viral life cycle during KSHV *de novo* infection and that its inhibition by GC7
326 potently blocks early events and prevents establishment of following persistent KSHV infection.

327

328 **Discussion**

329 Our innovative studies demonstrated that polyamine synthesis and eIF5A hypusination are
330 dynamically regulated by KSHV infection. We observed that intracellular polyamines are
331 overall upregulated in KSHV latently infected tumor cells by PolyamineRED staining (**Fig 1**).
332 However, the results from TLC assays have certain discrepancy likely due to that this type of

333 analysis only accesses to free polyamines and that disruption of cells may cause the significant
334 loss of polyamines as well. Nevertheless, TLC assays showed that spermine, the polyamine
335 species with the highest molecular weight, is still more abundant in KSHV latently infected
336 tumor cells. Impact of KSHV latency on polyamine synthesis could be explained by the fact
337 that the rate-limiting enzyme ODC1 is upregulated (**Fig 1**), since ODC1 is subjected to
338 transcriptional regulation of c-Myc [45, 46] that is upregulated by KSHV ORF73/LANA
339 protein dominantly expressed in KSHV latency [44]. Interestingly, spermidine is somehow
340 lowered in KSHV latently infected cells in TLC assays, which could be explained by
341 spermidine being consumed for the generation of hypusinated eIF5A that is indeed present at
342 higher level in KSHV latently infected cells (**Fig 5**). This may benefit the translation of KSHV
343 key latent protein ORF73/LANA, which is shown to depend on eIF5A hypusination in our own
344 studies (**Fig 6**). On the contrary, KSHV lytic reactivation triggers an overall decrease of
345 intracellular polyamines, particularly a dramatic depletion of spermidine (**Fig 1**), correlating
346 with the decrease of ODC1 during KSHV lytic reactivation (**Fig 1**) as well as the further
347 increase of hypusinated eIF5A in KSHV-reactivated cells (**Fig S5**). This is likely required to
348 fulfill the even higher demand of KSHV viral protein translation during lytic reactivation, since
349 the majority of KSHV genes (over 100) is expressed in lytic phase while only a dozen in latent
350 phase. We indeed showed that eIF5A hypusination is critical to translation of KSHV key lytic
351 protein ORF50/RTA (**Fig 6**). Other KSHV lytic proteins may also depend on hypusinated
352 eIF5A to translate, which needs further investigation. There could be also other explanations
353 for KSHV reactivation induced spermidine drop. For instance, polyamines are strongly charged
354 polycations, and it has been reported that spermidine and spermine are packed in HSV-1 virions
355 [21], allegedly to neutralize the negative charge of its large viral genomes and help with DNA
356 compaction. It still remains uncharacterized whether spermidine is also incorporated into
357 KSHV virion as HSV-1.

358 In these studies, we also clearly showed that polyamine synthesis and eIF5A hypusination
359 are critically required for KSHV infection. RNAi-mediated knockdown of several key enzymes
360 participating in polyamine synthesis, including ODC1, AGMAT, SRM, and SMS, unanimously
361 impairs KSHV lytic reactivation in multiple KSHV-infected cell systems (**Fig 2,3**), which is
362 further supported by the results that several chemical probes inhibiting polyamine synthesis,
363 including DFMO, clofazimine (CLF), and ribavirin, all block KSHV lytic reactivation in these
364 cells (**Fig 3,4**). Furthermore, our studies also innovatively identified that eIF5A hypusination is
365 the key linker to connect polyamine pathway with autophagy activation that is also critical to
366 KSHV viral infection, as we observed that ODC1 inhibitor DFMO indeed represses eIF5A
367 hypusination as well as autophagy activation that favors KSHV lytic switch (**Fig 5**). In addition,
368 a supportive finding is that knockdown of ODC1 seems to preferentially decrease spermidine
369 that is the key polyamine species utilized for eIF5A hypusination (**Fig 2**). Likewise, we
370 demonstrated that RNAi-mediated knockdown of the key enzyme DHPS participating in eIF5A
371 hypusination as well as its inhibition by GC7 both efficiently suppress KSHV lytic reactivation
372 in multiple KSHV-infected cell systems (**Fig 5, 7**). We further unraveled that one potential
373 mechanism is that translation of certain KSHV viral proteins could be hypusine-addicted (**Fig**
374 **6**), as activation of eIF5A depends on its hypusination by using spermidine [16], which enables
375 eIF5A to alleviate ribosome stalling on defined hard-to-translate tri-peptide motifs [17, 18]. We
376 indeed recognized that KSHV ORF50/RTA and ORF73/LANA proteins carry multiple of such
377 motifs that are conserved across all KSHV strains (**Fig 6, Table S1,2**). Beyond KSHV lytic
378 reactivation, inhibition of eIF5A hypusination by GC7 also impairs KSHV *de novo* infection,
379 likely through affecting synthesis of certain KSHV viral proteins possessing immune
380 antagonizing or cell proliferating functions which are required for early steps of KSHV
381 infection. For example, NF-κB is activated shortly post of KSHV *de novo* infection and
382 important to the establishment of latency [73].

383 By combining our new results with earlier knowledge regarding to host and viral controls
384 of KSHV infection, we propose the following model describing the comprehensive roles of
385 polyamine pathway and eIF5A hypusination in regulating KSHV viral infection (**Fig S8**). At
386 the latent phase of KSHV infection, LANA upregulates ODC1 expression while suppresses
387 RTA transcription [74]. ODC1 upregulation promotes intracellular polyamine biosynthesis
388 leading to an increase of spermine. In contrast, spermidine is actively and steadily consumed,
389 and hypusinated eIF5A is accumulated to further promote translation of LANA. At the early
390 stage of lytic switch, RTA transcription is activated, and the newly transcribed RTA mRNAs
391 can thus be efficiently translated thanks to the pre-existing higher level of hypusinated eIF5A.
392 RTA in turn promotes autophagy activation that would also benefit from increased hypusinated
393 eIF5A [19, 20], which overall favors KSHV lytic switch. However, at the late stage of lytic
394 phase, RTA expression is strong enough to counteract LANA, which leads to the reduction of
395 ODC1. Additionally, it has been shown that c-Myc expression is transcriptionally
396 downregulated by the KSHV lytic gene vIRF4 [48], which would also contribute to the decrease
397 of ODC1. ODC1 reduction decreases intracellular polyamines, and thus hamper cell cycle
398 progression [75], which has been shown to favor KSHV lytic reactivation [76]. In addition,
399 accumulated spermine would convert to spermidine and putrescine through SMOX and PAOX,
400 which further generates hydrogen peroxide and oxidative stress that have also been shown to
401 promote KSHV lytic reactivation [77, 78]. At this moment, KSHV lytic protein synthesis,
402 especially RTA, is already less dependent on hypusinated eIF5A, so decrease of intracellular
403 polyamines may generate much less adverse effect on KSHV lytic protein synthesis.
404 Additionally, the resulting attenuated autophagy would actually benefit the late phase of KSHV
405 lytic replication [79].

406 The evidence is emerging that KSHV modulates cellular metabolic landscape in order to
407 fulfill its particular needs to promote viral propagation and oncogenesis [37, 38]. A recent study

408 [39] reported that broad modifications of host metabolism, including induction of arginine and
409 proline metabolism, occur in KSHV-infected cells in 3D culture. Arginine is a precursor
410 metabolite for polyamine synthesis (**Fig 2A**), and it can be sequentially converted to putrescine
411 via ODC1 and AGAMT, both of which were identified as critical to KSHV lytic reactivation in
412 our studies (**Fig 2, 3**). Furthermore, these authors also reported that ornithine, the direct
413 substrate of ODC1, is induced in KSHV-infected cells, which resonates with our finding that
414 polyamines are upregulated by KSHV latent infection. Overall, these observations along with
415 ours illustrated that KSHV profoundly reprograms the metabolic pathways of host cells to not
416 only promote viral latency and oncogenesis but also favor viral lytic reactivation and
417 dissemination of KSHV viruses. However, it is still not fully clear how KSHV infection
418 modulates polyamine pathway and eIF5A hypusination. We believe that regulation of ODC1
419 by KSHV LANA might be just one of mechanisms. Some large DNA viruses encode functional
420 genes related to the polyamine metabolism, such as *Paramecium bursaria* chlorella virus
421 (PBCV-1) virus that encodes genes equivalent to most of the biosynthesis pathway [80-82] in
422 its 331-kb long genome. More recently, it has been reported that the viral genome of bovine
423 gammaherpesvirus BoVH-6 encodes a viral protein similar to ODC1 [83]. There are nearly 100
424 KSHV-encoded proteins, some of which may directly impact on polyamine pathway and eIF5A
425 hypusination. Such functions of certain KSHV proteins are pending for discovery.

426 After all, our understanding of polyamine pathway and eIF5A hypusination in the context
427 of KSHV infection will pave the way for development of new antiviral and antitumor strategies
428 to treat KSHV-associated malignancy. As the proof of principle in our studies, inhibitors
429 targeting polyamine pathway (DFMO, clofazimine, ribavirin) and eIF5A hypusination (GC7)
430 can be used as antivirals to block latent and lytic replications as well as *de novo* infection of
431 KSHV (**Fig S8**). As the matter of fact, three of them are already FDA-approved drugs currently
432 being prescribed for treating other diseases. Thus, these drugs are safe for future evaluation of

433 their potential to treat KSHV-associated malignancy in clinic. Beyond inhibition of KSHV
434 latent infection, interruption of KSHV lytic infection is equally important to not only block
435 generation of new KSHV virions and their dissemination but also reduce viral tumorigenesis
436 since KSHV lytic infection contributes notably to tumors as well by generating angiogenesis
437 and anti-apoptotic phenotypes (reviewed in [40, 41]). In conclusion, polyamine pathway and
438 eIF5A hypusination play a comprehensive role in regulating KSHV infections, which serve as
439 promising new drug targets for treating KSHV infection and KSHV-associated malignancy.

440

441 **Materials and Methods**

442 *Cell culture.* HEK293.r219 [50] and iSLK.BAC16 [42] cells were respectively obtained
443 from Dr. Prashant Desai (Johns Hopkins) and Dr. Shou-Jiang Gao (University of Pittsburgh)
444 and cultured in DMEM supplemented with 10% FBS under selection (HEK293.r219: 5 μg/mL
445 puromycin; iSLK.BAC16: 1.2 mg/mL Hygromycin B, 2 μg/mL puromycin, 250 μg/mL G418).
446 TREx BCBL1-RTA [84] cells were obtained from Dr. Jae Jung (Cleveland Clinic) and
447 maintained in RPMI supplemented with 10% FBS under selection (200 μg/mL Hygromycin B).
448 BC-3, BCBL1 and SLK cells were acquired from the NIH AIDS Reagent Program. These cells
449 were maintained in RPMI supplemented with 10% FBS (BC-3 with 20% FBS). BJAB and
450 Akata/BX cells were acquired from Dr. Renfeng Li (Virginia Commonwealth University) and
451 maintained in RPMI supplemented with 10% FBS (Akata/BX under selection 500μg/mL G418).
452 Tonsillar mononuclear cells and B lymphocytes were maintained in RPMI (Gibco)
453 supplemented with 10% heat-inactivated human serum (Advanced Biotechnologies Inc,
454 Cat#P2-203), 100 U/mL penicillin, 100 μg/mL streptomycin, 0.5 μg/mL Amphotericin B, and
455 50 μM β-Mercaptoethanol as previously described [85]. KSHV lytic reactivation was induced
456 in TREx BCBL1-RTA cells with 1μg/mL doxycycline, in iSLK.BAC16 cells with either

457 1μg/mL doxycycline alone or in combination with 1mM Sodium Butyrate (NaB), and in
458 HEK293.r219 cells with 20ng/mL 12-O-Tetradecanoylphorbol 13-acetate (TPA) and 0.3mM
459 NaB or ectopic expression of KSHV ORF50/RTA cDNA.

460 *Compounds.* 12-O-Tetradecanoylphorbol 13-acetate (Cat#P8139) and sodium butyrate
461 (Cat#AAA1107906) were purchased from Sigma-Aldrich and Fisher Scientific, respectively.
462 Doxycycline was obtained from Fisher Scientific (Cat#BP2653-1). Polyamine supplement
463 (1000x) (Cat#P8483), putrescine (Cat#P5780), spermidine (Cat#S0266), spermine
464 (Cat#S4264), and clofazimine (Cat# C8895) were purchased from Sigma-Aldrich. 2-
465 difluoromethylornithine (DFMO) (Cat#2761), ribavirin (Cat#R0077), and deoxyhypusine
466 synthase inhibitor N1-guanyl-1,7-diaminoheptane (GC7) (Cat#259545) were purchased from
467 Tocris, Tokyo Chemical Industry, and EMD Millipore respectively.

468 *Isolation of tonsillar B lymphocytes*. Tonsillar tissues were acquired through the National
469 Disease Research Interchange (NDRI, Philadelphia) and were collected from de-identified
470 healthy donors via routine tonsillectomy procedures. Extraction of mononuclear cells from the
471 tonsillar tissue was performed as previously described [85]. In brief, the block of tissue was cut
472 into smaller (3mm) pieces, and cells were mechanically dissociated by using a stainless-steel
473 sieve (250-μm mesh) with a syringe plunger, through which the tissue samples remained cold
474 and moistened in the Hanks balanced salt solution (HBSS) with antibiotics (100 U/mL
475 penicillin, 100 μg/mL streptomycin, 5 μg/mL gentamicin, 0.5 μg/mL Amphotericin B). Cell
476 suspension was passed through a 40 μm plastic cell strainer and overlaid onto 10 mL Ficoll-
477 Hypaque (GE Healthcare), followed by centrifugation (1000x g) for 20 mins at 4°C.
478 Mononuclear cells were collected from the buffy coat at the interface, and washed three times
479 with HBSS containing antibiotics and centrifuged (300x g) for 10mins at 4°C. Washed cells
480 were resuspended in cryopreservation media (HyClone, Cat#SR30001.02) mixed with tonsil

481 mononuclear cells complete media without antibiotics. B lymphocyte isolation was conducted
482 through negative selection by using the B cell Isolation Kit II (Miltenyi Biotec, Cat#130-091-
483 151) according to the manufacturer's protocol. Purity of B lymphocytes (>98%) was assessed
484 via immunostaining by using an anti-human-CD19, PE-conjugated antibody (Miltenyi Biotec,
485 Cat#130-113-731) per manufacturer's instructions and analyzed via flow cytometry on an
486 Accuri C6 Plus (BD Biosciences).

487 *Preparation of KSHV viruses and de novo infection*. iSLK.BAC16 cells were treated with
488 1µg/mL doxycycline and 1mM NaB for 24h, and then kept in fresh media only containing
489 1µg/mL doxycycline. Doxycycline was refreshed every 2 days. Supernatants were collected 6
490 dpi, centrifuged (400x g) for 10 mins to remove cellular debris, filtered through the 0.45µm
491 filter and stored at -80°C. KSHV BAC16 viruses were titrated in HEK293T cells through the
492 serial dilution of viral stock along with 8µg/mL polybrene via spinoculation (2500 rpm) for ~2h
493 at 37°C. Percentage of GFP-positive cells was determined by flow cytometry on an Accuri C6
494 Plus. Forward Scatter (FS) and Side Scatter (SS) were used for gating of single cells. Analysis
495 was performed using the FlowJo v10 software. Primary tonsillar B lymphocytes were
496 spinoculated (2500 rpm) with KSHV BAC16 viruses (MOI=3) along with 8µg/mL polybrene
497 for ~2h at 37°C. Cell media was completely removed at 12hpi. Unbound viruses were washed
498 away, and fresh media containing the tested compounds were added. Similarly, SLK cells were
499 subjected to KSHV *de novo* infection (MOI=0.5).

500 *Thin-layer chromatography*. Protocol of thin-layer chromatography (TLC) to analyze
501 polyamines was adapted from previous report [24, 86, 87]. Cells were harvested and
502 resuspended in 2% perchloric acid solution (v/v) in ddH2O (Cat#SP339-500), sonicated at 4°C
503 (30% amplitude, 1min total with 2sec ON and 2sec OFF), and incubated at 4°C for overnight
504 on a rotating shaker. Cell lysates were centrifuged (11500x g) for 45mins at 4°C, and transferred

505 to a new test tube. The following solutions were prepared freshly. 1 volume of cell lysates was
506 mixed with 2 volumes of dansyl-chloride solution (18.6mM in Acetone; Cat#D-2625,
507 Cat#BP392-100)) and 1 volume of supersaturated Sodium Carbonate solution (4.44M in
508 ddH2O; Cat#S263-500), which was vortexed thoroughly and incubated for overnight in dark
509 on a rotating shaker at room temperature. 0.5 volume of L-proline solution (1.3M in ddH2O;
510 Cat#BP392-100) was added, then samples were thoroughly vortexed and incubated for another
511 1h. For extraction of dansylated polyamines, 2.5 volume of toluene (Cat# AC610951000) was
512 added, and the mixtures were thoroughly vortexed and further incubated for 20 mins. The
513 mixtures were centrifuged (13500 rpm) for 10mins at room temperature. The organic phase
514 (upper layer) was carefully separated and spotted (~4uL) onto a TLC plate (Cat#1.05721.0001),
515 and individual polyamines were separated by ascending chromatography using a
516 cyclohexane:ethylacetate mixture (2:3) (v:v) as the eluant for 30 mins. Standards and controls
517 were processed identically in parallel. The TLC plate was then imaged by using a FluorChem
518 E (ProteinSimple) under UV light exposure.

519 *Cell transfection*. Reverse transfection of siRNA was performed using Lipofectamine
520 RNAiMAX (Invitrogen) as previously described [88]. Following Silencer Select siRNAs
521 (Invitrogen) were used: ornithine decarboxylase 1 (ODC1) (s9821, s9822, s9823 as si1-3),
522 agmatinase (AGMAT) (s379, s381 as si1-2), spermidine synthase (SMS) (s13173, s13175 as
523 si1-2), spermine synthase (SRM) (s13430, s13432 as si1-2), deoxyhypusine synthase (DHPS)
524 (s91, s92 as si1-2), and non-targeting control (Cat#AM4641). Turbofect (ThermoFisher) was
525 used for vector transfection following manufacturer's recommendations. Flag-tagged KSHV
526 ORF50/RTA vector was a gift from Dr. Pinghui Feng (University of South California) [89],
527 pSG5-BZLF1 was a gift from Dr. Diane Hayward (Addgene # 72637) [90], and pA3M-LANA
528 was a gift from Dr. Erle Robertson (University of Pennsylvania). The pmaxGFP plasmid was
529 obtained from Lonza.

530 *Immunoblotting*. Protein immunoblotting was performed as previously described [91]. The
531 following antibodies were used: anti-ODC1 (EMD Millipore, Cat#MABS36), anti-hypusine-
532 eIF5A (EMD Millipore, Cat#ABS1064), anti-SSAT-1 (Novus, Cat#NB110-41622), anti-
533 LC3I/II (CST, Cat#4108), anti-SQSTM1/p62 (D5E2) (CST, Cat#8025), anti-GAPDH (SCBT,
534 Cat#sc-47724), anti-β-actin (SCBT, Cat#sc-47778), anti-DHPS (SCBT, Cat#sc-365077), anti-
535 EBV-ZEBRA/Zta (SCBT, Cat#sc-53904), anti-HHV8-K8.1A/B (SCBT, Cat#sc-65446), anti-
536 HHV8-ORF50/RTA (Abbiotec, Cat#251345), anti-KSHV-ORF26 (2F6B8) (Novus,
537 Cat#NBP1-47357), anti-KSHV-LANA (Advanced Biotechnologies, cat# 13-210-100), anti-
538 FLAG (CST, Cat#14793), anti-mouse-HRP (Invitrogen, Cat# 31430), anti-rabbit-HRP
539 (Invitrogen, Cat#A27036), anti-rat-HRP (Invitrogen, Cat#A18739). An anti-KSHV-ORF45
540 antibody was a gift from Dr. Fanxiu Zhu (Florida State University).

541 *Real-Time quantitative PCR*. The procedures of RNA extraction, cDNA preparation,
542 genomic DNA extraction, and real-time quantitative PCR (RT-qPCR) assays were conducted
543 as previously described [88]. Primers used in this study are listed in **Table S3**.

544 *Cell viability*. CellTiter-Glo (Promega, Cat# G7570) was used for cell viability assays
545 following the manufacturer's instructions. Luminescence was measured on a BioTeK Cytation
546 5 plate reader.

547 *Confocal and fluorescence microscopy*. SLK and iSLK.BAC16 cells were seeded onto the
548 high precision cover glasses (Bioscience Tools, Cat#CSHP-No1.5-13) pre-coated with poly-L-
549 lysine (R&D Systems, Cat#3438-100-01) for 45mins in a 24-well plate. These cells were
550 induced with 1μg/mL doxycycline for 48h, and incubated with fresh media containing 10mM
551 Polyamine Red (Funakoshi, Cat#FDV-0020) for 15mins. The following steps were all
552 performed in dark. Cells were rinsed and fixed with 4% paraformaldehyde for 8 mins at room
553 temperature, followed by staining with Hoechst (Invitrogen) per manufacturer's guidelines.

554 Coverslips were rinsed and mounted on slides by using ProLong Glass Antifade Mountant
555 (Invitrogen, Cat#P36982). Slides were left to cure in dark for 24h at room temperature per
556 manufacturer's recommendations. Confocal images were acquired by using the ZEISS LSM
557 700 Upright laser scanning confocal microscope and ZEN imaging software (ZEISS).
558 Polyamines were imaged via TAMRA channel [43], while GFP is constitutively expressed in
559 cells infected with KSHV BAC16 [42]. Image analysis was performed by using the ImageJ
560 software. For BJAB and BCBL-1 cells, the procedure was similar with slight modifications:
561 The suspended cells (4 x10^4 cells/mL) were incubated with 10mM PolyamineRED (Funakoshi
562 Co.,Ltd) for 15 mins, and washed 2 times with 1x PBS. Cells were fixed and subjected to
563 Hoechst staining, followed by the PBS washing. These cells were spun down onto the poly-L-
564 lysine-coated high precision cover glasses in 24-well plates via brief centrifugation (2000 rpm)
565 for 2mins. Cover glasses were mounted and analyzed as above. Fluorescence images of
566 HEK293.r219 cells at GFP and RFP channels as well as SLK cells *de novo* infected with KSHV
567 BAC16 viruses at GFP channel were acquired by using a BioTeK Cytation 5 plate reader.
568 Hoechst was used to stain nuclei.

569 *Protein sequence scanning*. Protein sequences were retrieved from the NCBI database and
570 scanned for hyp-eIF5A-dependent pause motifs [17] by using the ScanProsite webtool
571 (https://prosite.expasy.org/prosite.html) [92].

572 *Statistical analysis*. Statistical analysis was performed by using GraphPad PRISM 5 or
573 Excel. Results were presented as mean ± SEM. p-values were determined by using the two-
574 tailed paired Student t-test.

575

576 **Acknowledgments**

We would like to thank Drs Prashant Desai, Jae Jung, Shou-Jiang Gao, Renfeng Li for the gifts of HEK293.r219, TREx BCBL1-RTA, iSLK.BAC16, and Akata/BX cells. SLK and BCBL-1 cells were acquired through the NIH AIDS Reagent Program thanks to Drs. Jay A. Levy and Sophie Leventon-Kriss for SLK, and Drs. Michael McGrath and Don Ganem for BCBL-1. We would like to thank Drs Pinghui Feng, Erle Robertson, and Diane Hayward for the gifts of Flag-tagged KSHV-ORF50/RTA, pA3M-LANA, and pSG5-BZLF1 vectors. We would also like to thank Dr. Fanxiu Zhu for the gift of anti-KSHV-ORF45 antibody.

Author contributions: J.Z., G.F. conceived the study. G.F. performed experiments. G.F., J.Z., N.S. analyzed data and wrote the manuscript. A.B., D.Z., W.K., and M.J. provided reagents, technical support, or comments of this study. J.Z. provided overall supervision of the study.

Funding

This work was supported by grants to J.Z. (R01DE025447, R01AI150448) and N.S. (R03DE029716) from the National Institute of Health.

Conflict of Interest Statement: Authors declare that research was conducted in absence of any potential conflict of interest.

Data Availability statement: The authors declare that all relevant data supporting the study can be found within the manuscript or the supplementary information.

599 **References**

600 1. Watanabe, S. et al. (1991) Estimation of polyamine binding to macromolecules and ATP in
601 bovine lymphocytes and rat liver. J Biol Chem 266 (31), 20803-9.
602 2. Celano, P. et al. (1989) Polyamines differentially modulate the transcription of growth-
603 associated genes in human colon carcinoma cells. J Biol Chem 264 (15), 8922-7.
604 3. Frugier, M. et al. (1994) Synthetic polyamines stimulate in vitro transcription by T7 RNA
605 polymerase. Nucleic Acids Res 22 (14), 2784-90.
606 4. Gallo, C.J. et al. (1986) Polyamines and HeLa-cell DNA replication. Biochem J 238 (1), 37-
607 42.
608 5. Yamashita, T. et al. (2013) Role of polyamines at the G1/S boundary and G2/M phase of the
609 cell cycle. Int J Biochem Cell Biol 45 (6), 1042-50.
610 6. Pasini, A. et al. (2014) Chromatin remodeling by polyamines and polyamine analogs. Amino
611 Acids 46 (3), 595-603.
612 7. Nakajima, K.I. et al. (2015) KCNJ15/Kir4.2 couples with polyamines to sense weak
613 extracellular electric fields in galvanotaxis. Nat Commun 6, 8532.
614 8. Coffino, P. (2001) Regulation of cellular polyamines by antizyme. Nat Rev Mol Cell Biol 2
615 (3), 188-94.
616 9. Pegg, A.E. (2006) Regulation of ornithine decarboxylase. J Biol Chem 281 (21), 14529-32.
617 10. Arruabarrena-Aristorena, A. et al. (2018) Oil for the cancer engine: The cross-talk between
618 oncogenic signaling and polyamine metabolism. Sci Adv 4 (1), eaar2606.
619 11. Casero, R.A., Jr. et al. (2018) Polyamine metabolism and cancer: treatments, challenges and
620 opportunities. Nat Rev Cancer 18 (11), 681-695.
621 12. Fujimura, K. et al. (2014) A hypusine-eIF5A-PEAK1 switch regulates the pathogenesis of
622 pancreatic cancer. Cancer Res 74 (22), 6671-81.
623 13. Memin, E. et al. (2014) Blocking eIF5A modification in cervical cancer cells alters the
624 expression of cancer-related genes and suppresses cell proliferation. Cancer Res 74 (2), 552-
625 62.
626 14. Muramatsu, T. et al. (2016) The hypusine cascade promotes cancer progression and
627 metastasis through the regulation of RhoA in squamous cell carcinoma. Oncogene 35 (40),
628 5304-5316.
629 15. Shiba, T. et al. (1971) Hypusine, a new amino acid occurring in bovine brain. Isolation and
630 structural determination. Biochim Biophys Acta 244 (3), 523-31.
631 16. Dever, T.E. et al. (2014) The hypusine-containing translation factor eIF5A. Crit Rev
632 Biochem Mol Biol 49 (5), 413-25.
633 17. Schuller, A.P. et al. (2017) eIF5A Functions Globally in Translation Elongation and
634 Termination. Mol Cell 66 (2), 194-205 e5.
635 18. Huter, P. et al. (2017) Structural Basis for Polyproline-Mediated Ribosome Stalling and
636 Rescue by the Translation Elongation Factor EF-P. Mol Cell 68 (3), 515-527 e6.
637 19. Lubas, M. et al. (2018) eIF5A is required for autophagy by mediating ATG3 translation.
638 EMBO Rep 19 (6).
639 20. Zhang, H. et al. (2019) Polyamines Control eIF5A Hypusination, TFEB Translation, and
640 Autophagy to Reverse B Cell Senescence. Mol Cell 76 (1), 110-125 e9.
641 21. Gibson, W. and Roizman, B. (1971) Compartmentalization of spermine and spermidine in
642 the herpes simplex virion. Proc Natl Acad Sci U S A 68 (11), 2818-21.
643 22. Lanzer, W. and Holowczak, J.A. (1975) Polyamines in vaccinia virions and polypeptides
644 released from viral cores by acid extraction. J Virol 16 (5), 1254-64.
645 23. Fout, G.S. et al. (1984) Radiochemical determination of polyamines in poliovirus and
646 human rhinovirus 14. J Biol Chem 259 (6), 3639-43.

647 24. Mounce, B.C. et al. (2016) Interferon-Induced Spermidine-Spermine Acetyltransferase and
648 Polyamine Depletion Restrict Zika and Chikungunya Viruses. Cell Host Microbe 20 (2), 167-
649 77.
650 25. Olsen, M.E. et al. (2018) Differential Mechanisms for the Involvement of Polyamines and
651 Hypusinated eIF5A in Ebola Virus Gene Expression. J Virol 92 (20).
652 26. Olsen, M.E. et al. (2016) Polyamines and Hypusination Are Required for Ebolavirus Gene
653 Expression and Replication. mBio 7 (4).
654 27. Mastrodomenico, V. et al. (2019) Polyamine Depletion Inhibits Bunyavirus Infection via
655 Generation of Noninfectious Interfering Virions. J Virol 93 (14).
656 28. Mastrodomenico, V. et al. (2020) Virion-Associated Polyamines Transmit with
657 Bunyaviruses to Maintain Infectivity and Promote Entry. ACS Infect Dis 6 (9), 2490-2501.
658 29. Isom, H.C. (1979) Stimulation of ornithine decarboxylase by human cytomegalovirus. J
659 Gen Virol 42 (2), 265-78.
660 30. Tyms, A.S. and Williamson, J.D. (1982) Inhibitors of polyamine biosynthesis block human
661 cytomegalovirus replication. Nature 297 (5868), 690-1.
662 31. Greco, A. et al. (2005) S-adenosyl methionine decarboxylase activity is required for the
663 outcome of herpes simplex virus type 1 infection and represents a new potential therapeutic
664 target. FASEB J 19 (9), 1128-30.
665 32. Shi, M. et al. (2013) Downregulation of the polyamine regulator spermidine/spermine N(1)-
666 acetyltransferase by Epstein-Barr virus in a Burkitt's lymphoma cell line. Virus Res 177 (1),
667 11-21.
668 33. Chang, Y. et al. (1994) Identification of herpesvirus-like DNA sequences in AIDS-
669 associated Kaposi's sarcoma. Science 266 (5192), 1865-9.
670 34. Moore, P.S. and Chang, Y. (1995) Detection of herpesvirus-like DNA sequences in Kaposi's
671 sarcoma in patients with and those without HIV infection. N Engl J Med 332 (18), 1181-5.
672 35. Cesarman, E. et al. (1995) Kaposi's sarcoma-associated herpesvirus-like DNA sequences in
673 AIDS-related body-cavity-based lymphomas. N Engl J Med 332 (18), 1186-91.
674 36. Soulier, J. et al. (1995) Kaposi's sarcoma-associated herpesvirus-like DNA sequences in
675 multicentric Castleman's disease. Blood 86 (4), 1276-80.
676 37. Delgado, T. et al. (2010) Induction of the Warburg effect by Kaposi's sarcoma herpesvirus
677 is required for the maintenance of latently infected endothelial cells. Proc Natl Acad Sci U S A
678 107 (23), 10696-701.
679 38. Lagunoff, M. (2016) Activation of cellular metabolism during latent Kaposi's Sarcoma
680 herpesvirus infection. Curr Opin Virol 19, 45-9.
681 39. Choi, U.Y. et al. (2020) Oncogenic human herpesvirus hijacks proline metabolism for
682 tumorigenesis. Proc Natl Acad Sci U S A 117 (14), 8083-8093.
683 40. Manners, O. et al. (2018) Contribution of the KSHV and EBV lytic cycles to
684 tumourigenesis. Curr Opin Virol 32, 60-70.
685 41. Jha, H.C. et al. (2016) The Role of Gammaherpesviruses in Cancer Pathogenesis. Pathogens
686 5 (1).
687 42. Brulois, K.F. et al. (2012) Construction and manipulation of a new Kaposi's sarcoma-
688 associated herpesvirus bacterial artificial chromosome clone. J Virol 86 (18), 9708-20.
689 43. Vong, K.K.H. et al. (2017) Cancer cell targeting driven by selective polyamine reactivity
690 with glycine propargyl esters. Chem Commun (Camb) 53 (60), 8403-8406.
691 44. Liu, J. et al. (2007) The Kaposi's sarcoma-associated herpesvirus LANA protein stabilizes
692 and activates c-Myc. J Virol 81 (19), 10451-9.
693 45. Bello-Fernandez, C. et al. (1993) The ornithine decarboxylase gene is a transcriptional
694 target of c-Myc. Proc Natl Acad Sci U S A 90 (16), 7804-8.
695 46. Pena, A. et al. (1993) Regulation of human ornithine decarboxylase expression by the c-
696 Myc.Max protein complex. J Biol Chem 268 (36), 27277-85.

697 47. Park, A. et al. (2020) Global epigenomic analysis of KSHV-infected primary effusion
698 lymphoma identifies functional MYC superenhancers and enhancer RNAs. Proc Natl Acad Sci
699 U S A 117 (35), 21618-21627.
700 48. Lee, H.R. et al. (2014) Kaposi's sarcoma-associated herpesvirus viral interferon regulatory
701 factor 4 (vIRF4) targets expression of cellular IRF4 and the Myc gene to facilitate lytic
702 replication. J Virol 88 (4), 2183-94.
703 49. Myoung, J. and Ganem, D. (2011) Active lytic infection of human primary tonsillar B cells
704 by KSHV and its noncytolytic control by activated CD4+ T cells. J Clin Invest 121 (3), 1130-
705 40.
706 50. Vieira, J. and O'Hearn, P.M. (2004) Use of the red fluorescent protein as a marker of
707 Kaposi's sarcoma-associated herpesvirus lytic gene expression. Virology 325 (2), 225-40.
708 51. Horyn, O. et al. (2005) Biosynthesis of agmatine in isolated mitochondria and perfused rat
709 liver: studies with 15N-labelled arginine. Biochem J 388 (Pt 2), 419-25.
710 52. Wang, X. et al. (2014) Arginine decarboxylase and agmatinase: an alternative pathway for
711 de novo biosynthesis of polyamines for development of mammalian conceptuses. Biol Reprod
712 90 (4), 84.
713 53. Tate, P.M. et al. (2019) Ribavirin Induces Polyamine Depletion via Nucleotide Depletion
714 to Limit Virus Replication. Cell Rep 28 (10), 2620-2633 e4.
715 54. Fairlamb, A.H. (2003) Chemotherapy of human African trypanosomiasis: current and future
716 prospects. Trends Parasitol 19 (11), 488-94.
717 55. Sholler, G.L.S. et al. (2018) Maintenance DFMO Increases Survival in High Risk
718 Neuroblastoma. Sci Rep 8 (1), 14445.
719 56. Lewis, E.C. et al. (2020) A subset analysis of a phase II trial evaluating the use of DFMO
720 as maintenance therapy for high-risk neuroblastoma. Int J Cancer.
721 57. Alexiou, G.A. et al. (2017) Difluoromethylornithine in cancer: new advances. Future Oncol
722 13 (9), 809-819.
723 58. Bianchi-Smiraglia, A. et al. (2018) Inhibition of the aryl hydrocarbon receptor/polyamine
724 biosynthesis axis suppresses multiple myeloma. J Clin Invest 128 (10), 4682-4696.
725 59. Nahid, P. et al. (2019) Treatment of Drug-Resistant Tuberculosis. An Official
726 ATS/CDC/ERS/IDSA Clinical Practice Guideline. Am J Respir Crit Care Med 200 (10), e93-
727 e142.
728 60. Rossi, D. et al. (2014) eIF5A and EF-P: two unique translation factors are now traveling the
729 same road. Wiley Interdiscip Rev RNA 5 (2), 209-22.
730 61. Wen, H.J. et al. (2010) Enhancement of autophagy during lytic replication by the Kaposi's
731 sarcoma-associated herpesvirus replication and transcription activator. J Virol 84 (15), 7448-
732 58.
733 62. Hung, C.H. et al. (2014) Regulation of autophagic activation by Rta of Epstein-Barr virus
734 via the extracellular signal-regulated kinase pathway. J Virol 88 (20), 12133-45.
735 63. Vanrell, M.C. et al. (2013) Polyamine depletion inhibits the autophagic response
736 modulating Trypanosoma cruzi infectivity. Autophagy 9 (7), 1080-93.
737 64. Eisenberg, T. et al. (2009) Induction of autophagy by spermidine promotes longevity. Nat
738 Cell Biol 11 (11), 1305-14.
739 65. Chauhan, S. et al. (2015) IRGM governs the core autophagy machinery to conduct
740 antimicrobial defense. Mol Cell 58 (3), 507-21.
741 66. Petkova, D.S. et al. (2012) IRGM in autophagy and viral infections. Front Immunol 3, 426.
742 67. Wohlgemuth, I. et al. (2008) Modulation of the rate of peptidyl transfer on the ribosome by
743 the nature of substrates. J Biol Chem 283 (47), 32229-35.
744 68. Woolstenhulme, C.J. et al. (2015) High-precision analysis of translational pausing by
745 ribosome profiling in bacteria lacking EFP. Cell Rep 11 (1), 13-21.

746 69. Ude, S. et al. (2013) Translation elongation factor EF-P alleviates ribosome stalling at
747 polyproline stretches. Science 339 (6115), 82-5.
748 70. Nakanishi, S. and Cleveland, J.L. (2016) Targeting the polyamine-hypusine circuit for the
749 prevention and treatment of cancer. Amino Acids 48 (10), 2353-62.
750 71. Schultz, C.R. et al. (2018) Synergistic drug combination GC7/DFMO suppresses
751 hypusine/spermidine-dependent eIF5A activation and induces apoptotic cell death in
752 neuroblastoma. Biochem J 475 (2), 531-545.
753 72. Jakus, J. et al. (1993) Features of the spermidine-binding site of deoxyhypusine synthase as
754 derived from inhibition studies. Effective inhibition by bis- and mono-guanylated diamines and
755 polyamines. J Biol Chem 268 (18), 13151-9.
756 73. Sadagopan, S. et al. (2007) Kaposi's sarcoma-associated herpesvirus induces sustained NF-
757 kappaB activation during de novo infection of primary human dermal microvascular endothelial
758 cells that is essential for viral gene expression. J Virol 81 (8), 3949-68.
759 74. Lu, F. et al. (2006) Acetylation of the latency-associated nuclear antigen regulates
760 repression of Kaposi's sarcoma-associated herpesvirus lytic transcription. J Virol 80 (11), 5273-
761 82.
762 75. Ray, R.M. et al. (1999) Polyamine depletion arrests cell cycle and induces inhibitors
763 p21(Waf1/Cip1), p27(Kip1), and p53 in IEC-6 cells. Am J Physiol 276 (3), C684-91.
764 76. Balistreri, G. et al. (2016) Oncogenic Herpesvirus Utilizes Stress-Induced Cell Cycle
765 Checkpoints for Efficient Lytic Replication. PLoS Pathog 12 (2), e1005424.
766 77. Li, X. et al. (2011) Oxidative stress induces reactivation of Kaposi's sarcoma-associated
767 herpesvirus and death of primary effusion lymphoma cells. J Virol 85 (2), 715-24.
768 78. Ye, F. et al. (2011) Reactive oxygen species hydrogen peroxide mediates Kaposi's sarcoma-
769 associated herpesvirus reactivation from latency. PLoS Pathog 7 (5), e1002054.
770 79. Cirone, M. (2018) EBV and KSHV Infection Dysregulates Autophagy to Optimize Viral
771 Replication, Prevent Immune Recognition and Promote Tumorigenesis. Viruses 10 (11).
772 80. Baumann, S. et al. (2007) Chlorella viruses contain genes encoding a complete polyamine
773 biosynthetic pathway. Virology 360 (1), 209-17.
774 81. Morehead, T.A. et al. (2002) Ornithine decarboxylase encoded by chlorella virus PBCV-1.
775 Virology 301 (1), 165-75.
776 82. Charlop-Powers, Z. et al. (2012) Paramecium bursaria chlorella virus 1 encodes a polyamine
777 acetyltransferase. J Biol Chem 287 (12), 9547-51.
778 83. Jia, J. et al. (2014) Novel gammaherpesvirus functions encoded by bovine herpesvirus 6
779 (bovine lymphotropic virus). J Gen Virol 95 (Pt 8), 1790-1798.
780 84. Nakamura, H. et al. (2003) Global changes in Kaposi's sarcoma-associated virus gene
781 expression patterns following expression of a tetracycline-inducible Rta transactivator. J Virol
782 77 (7), 4205-20.
783 85. Johnston, A. et al. (2009) Isolation of mononuclear cells from tonsillar tissue. Curr Protoc
784 Immunol Chapter 7, Unit 7 8.
785 86. Madhubala, R. (1998) Thin-layer chromatographic method for assaying polyamines.
786 Methods Mol Biol 79, 131-6.
787 87. Bartzatt, R. (2001) Fluorescent labeling of drugs and simple organic compounds containing
788 amine functional groups, utilizing dansyl chloride in Na(2)CO(3) buffer. J Pharmacol Toxicol
789 Methods 45 (3), 247-53.
790 88. Fiches, G.N. et al. (2020) Profiling of immune related genes silenced in EBV-positive
791 gastric carcinoma identified novel restriction factors of human gammaherpesviruses. PLoS
792 Pathog 16 (8), e1008778.
793 89. Li, J. et al. (2019) Antiviral activity of a purine synthesis enzyme reveals a key role of
794 deamidation in regulating protein nuclear import. Sci Adv 5 (10), eaaw7373.

90. Sarisky, R.T. et al. (1996) A replication function associated with the activation domain of the Epstein-Barr virus Zta transactivator. J Virol 70 (12), 8340-7.
91. Zhou, D. et al. (2020) Inhibition of Polo-like kinase 1 (PLK1) facilitates the elimination of HIV-1 viral reservoirs in CD4(+) T cells ex vivo. Sci Adv 6 (29), eaba1941.
92. de Castro, E. et al. (2006) ScanProsite: detection of PROSITE signature matches and ProRule-associated functional and structural residues in proteins. Nucleic Acids Res 34 (Web Server issue), W362-5.

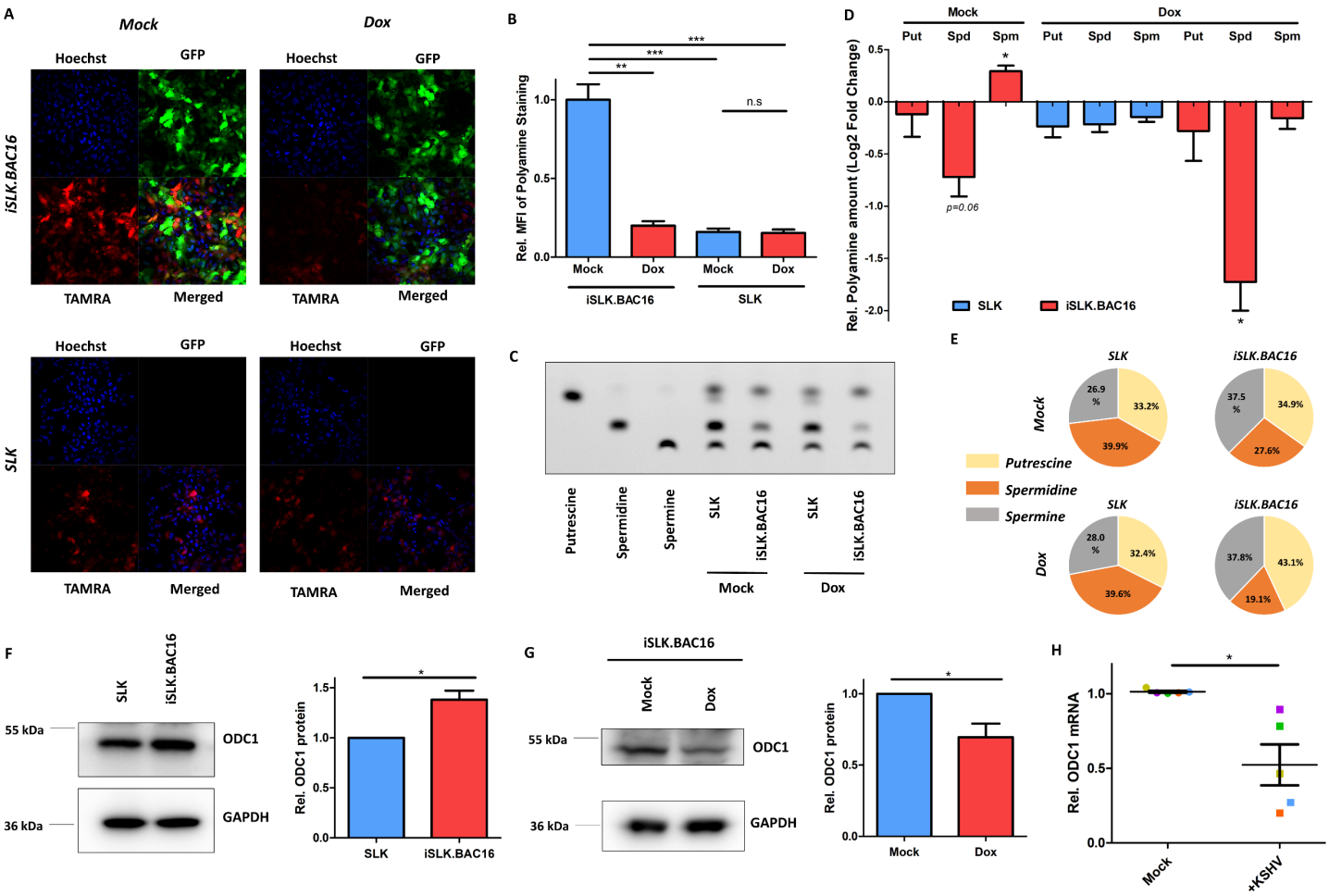

803

804 **Figure 1. KSHV dynamically modulates the level of intracellular polyamines.** (A, B).
805 Intracellular polyamines in SLK and iSLK.BAC16 cells treated with doxycycline (Dox;
806 1µg/mL) for 48h or mock were stained with PolyamineRED (TAMRA) and visualized by
807 confocal fluorescence microscopy (A), whereas nuclei were labelled with Hoechst (Blue). GFP
808 is constitutively expressed in cells infected with KSHV BAC16. Mean fluorescence intensity
809 (MFI) of polyamine fluorescence signal (TAMRA) of ≥ 1500 cells (B) was determined and
810 normalized to mock-treated iSLK.BAC16 cells. (C-E). Intracellular polyamine species
811 (putrescine [Put], spermidine [Spd], spermine [Spm]) in SLK and iSLK.BAC16 cells treated
812 with Dox for 48h or mock were analyzed by thin-layer chromatography (TLC) with pure
813 individual polyamine species used as reference (C). Relative changes of polyamine species (Put,

814 Spd, Spm) in TLC results were determined and normalized to mock-treated SLK cells (D), or
815 displayed as the relative proportion of total intracellular polyamines in pie chart (E). (F, G).
816 ODC1 protein in SLK and iSLK.BAC16 cells (F) as well as in iSLK.BAC16 cells treated with
817 Dox or mock (G) was measured by immunoblotting. Intensity of protein bands was determined
818 by using AlphaView SA (software) and normalized to GAPDH. (H) Primary tonsillar B
819 lymphocytes from 5 healthy donors were isolated and infected with KSHV BAC16 viruses or
820 mock treated. mRNA level of ODC1 in these cells at 3 dpi was measured by RT-qPCR assays
821 and normalized to mock treatment. Results were calculated from n=3-4 independent
822 experiments and presented as mean ± SEM (* $p<0.05$; ** $p<0.01$; *** $p<0.001$, two-tailed
823 paired Student t-test).
824

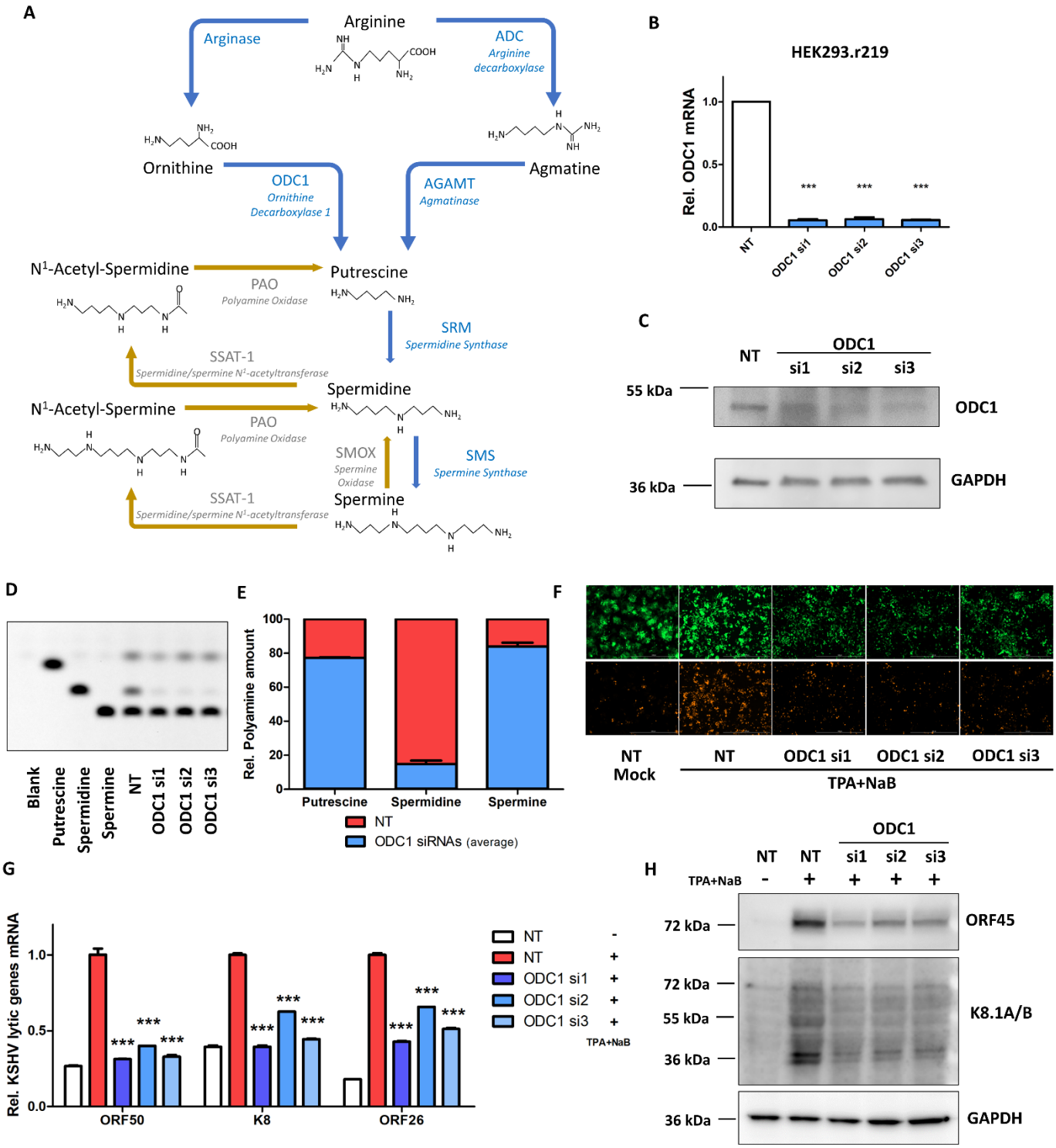

825

826 **Figure 2. ODC1 is required for KSHV lytic reactivation.** (A). Schematic view of the

827 polyamine biosynthesis pathway. (B, C). ODC1 knockdown in HEK293.r219 cells transfected

828 with ODC1 siRNAs (si1, si2, si3) or non-targeting control siRNA (NT) was analyzed by RT-
829 qPCR (B) or immunoblotting (C). (D, E). Intracellular polyamine species (Put, Spd, Spm) in
830 HEK293.r219 cells transfected with ODC1 siRNAs (si1, si2, si3) or NT were analyzed by TLC
831 with pure individual polyamine species used as reference (D). Relative polyamine species (Put,
832 Spd, Spm) in above cells were quantified (average of ODC1 si1-3) and normalized to NT-
833 transfected cells. Results were calculated from n=2 independent repeats. (F-H). HEK293.r219
834 cells transfected with ODC1 siRNAs (si1, si2, si3) or NT were treated with TPA (20 ng/mL) +
835 NaB (0.3mM) for 48h, and visualized by fluorescence imaging (F). Expression of RFP protein
836 indicates KSHV lytic reactivation, while GFP signal means that cells are KSHV-infected.
837 mRNA level of KSHV lytic genes (ORF50/RTA, K8/K-bZIP, ORF26) in above cells was
838 analyzed by RT-qPCR assays and normalized to NT-transfected induced cells (G). Protein level
839 of KSHV lytic genes (ORF45, K8.1A/B) was analyzed by immunoblotting assays (H). GAPDH
840 was used as the loading control. Results were calculated from n=3 independent experiments
841 and presented as mean ± SEM (* $p<0.05$; ** $p<0.01$; *** $p<0.001$, two-tailed paired Student t-
842 test).
843

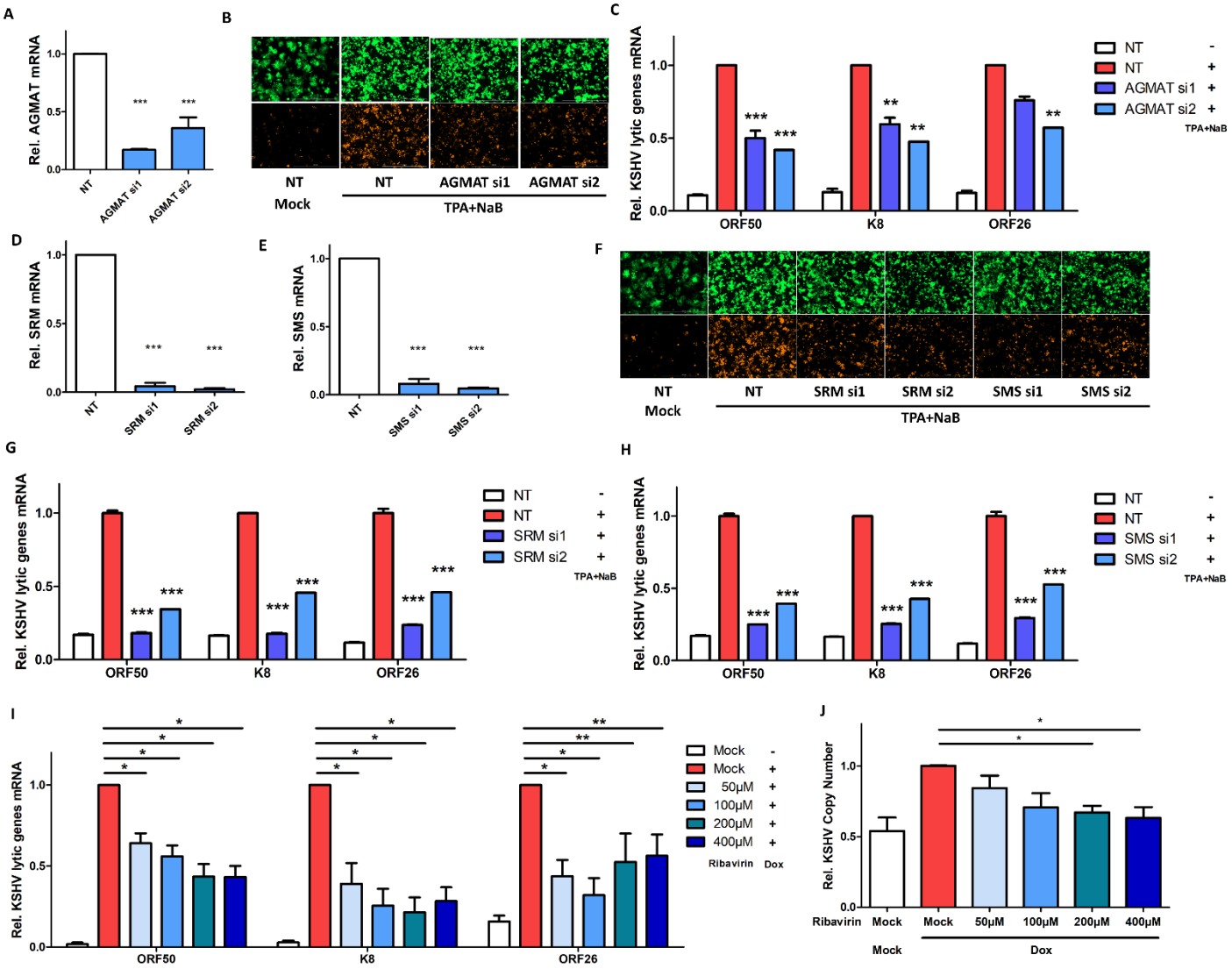

Figure 3. Other polyamine enzymes contribute to KSHV lytic reactivation. (A-C) AGMAT knockdown in HEK293.r219 cells transfected with AGMAT siRNAs (si1, si2) or NT was analyzed by RT-qPCR assays (A). HEK293.r219 cells transfected with AGMAT siRNAs (si1, si2) or NT was treated with TPA (20 ng/mL) + NaB (0.3mM) for 48h, and visualized by fluorescence imaging (B). mRNA level of KSHV lytic genes (ORF50/RTA, K8/K-bZIP, ORF26) in above cells was analyzed by RT-qPCR assays and normalized to NT-transfected induced cells (C). (D, E). SRM (D) or SMS (E) knockdown in HEK293.r219 cells transfected with their siRNAs (si1, si2) or NT was analyzed by RT-qPCR assays. (F-H). HEK293.r219

853 cells transfected with SRM/SMS siRNAs (si1, si2) or NT was treated with TPA (20 ng/mL) +
854 NaB (0.3mM) for 48h, and visualized by fluorescence imaging (F). mRNA level of KSHV lytic
855 genes (ORF50/RTA, K8/K-bZIP, ORF26) in SRM (G) or SMS (H) depleted, TPA+NaB-
856 induced HEK293.r219 cells was analyzed by RT-qPCR assays and normalized to NT-
857 transfected induced cells. (I, J). mRNA level of KSHV lytic genes (ORF50/RTA, K8/K-bZIP,
858 ORF26) in iSLK.BAC16 cells pretreated with increasing doses of ribavirin for 24h and
859 subsequently induced with Dox (1μg/mL) was analyzed by RT-qPCR assays (I). Copy number
860 of KSHV genomes in above cells was also analyzed (J). Results were calculated from n=3
861 independent experiments and presented as mean ± SEM (* $p<0.05$; ** $p<0.01$; *** $p<0.001$,
862 two-tailed paired Student t-test).
863

A

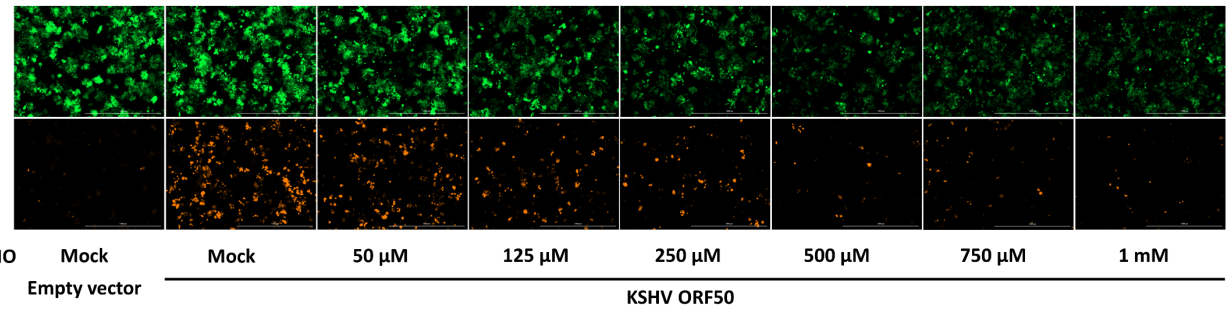
DFMO
Mock
Mock
50 μM
125 μM
250 μM
500 μM
750 μM
1 mM
Empty vector
KSHV ORF50

B

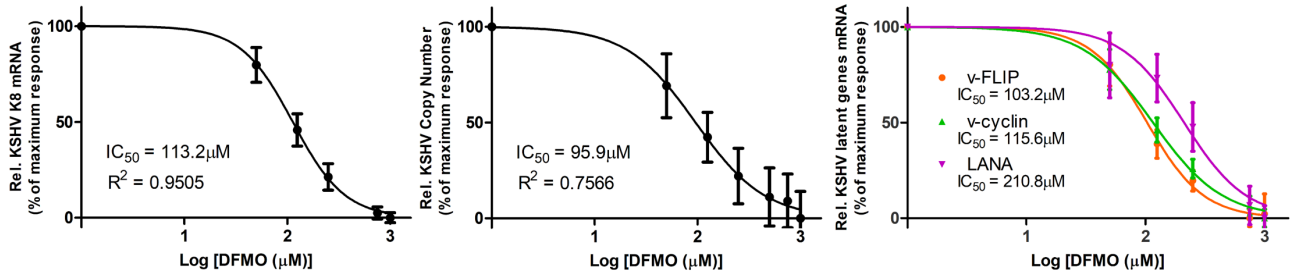
Rel. KSHV K8 mRNA (% of maximum response)
IC50 = 113.2μM
R2 = 0.9505
Log [DFMO (μM)]
Rel. KSHV Copy Number (% of maximum response)
IC50 = 95.9μM
R2 = 0.7566
Log [DFMO (μM)]
Rel. KSHV latent genes mRNA (% of maximum response)
v-FLIP IC50 = 103.2μM
v-cyclin IC50 = 115.6μM
LANA IC50 = 210.8μM
Log [DFMO (μM)]

C

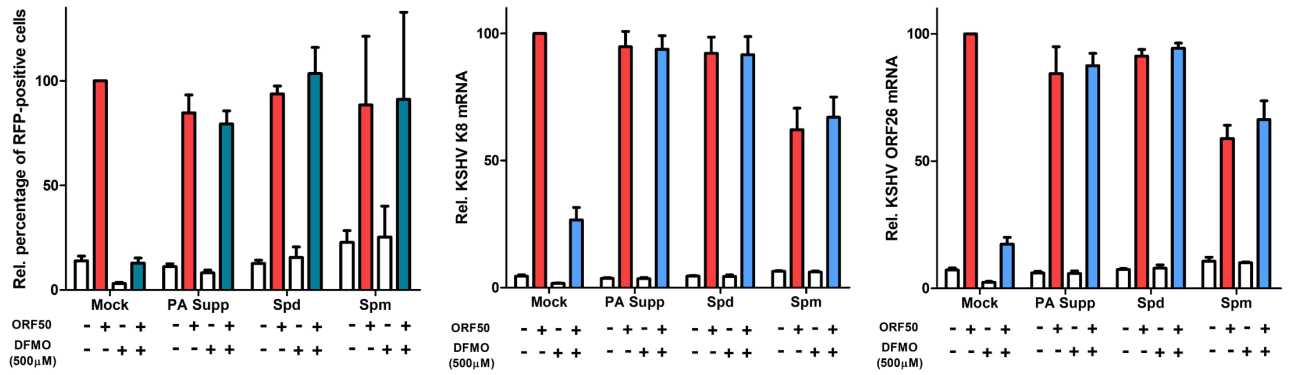
Rel. percentage of RFP-positive cells
Rel. KSHV K8 mRNA
Rel. KSHV ORF26 mRNA
Mock
PA Supp
Spd
Spm
ORF50
DFMO (500μM)

D

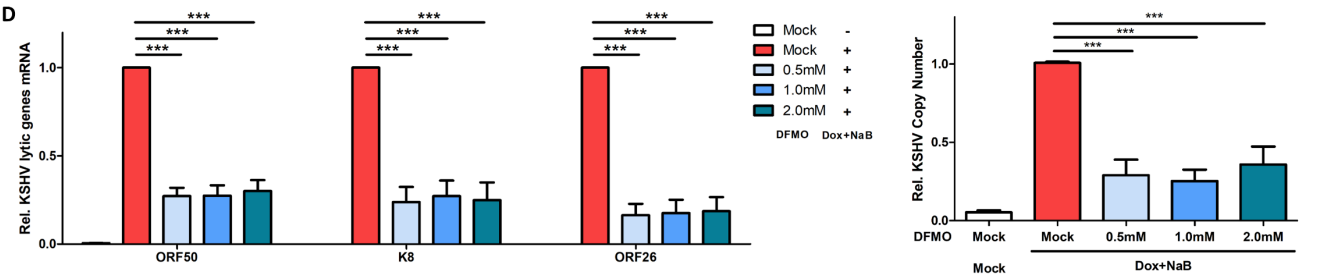
Rel. KSHV lytic genes mRNA
ORF50
K8
ORF26
Mock
Mock
0.5mM
1.0mM
2.0mM
DFMO
Dox+NaB
Rel. KSHV Copy Number
DFMO
Mock
Mock
0.5mM
1.0mM
2.0mM
Dox+NaB

E

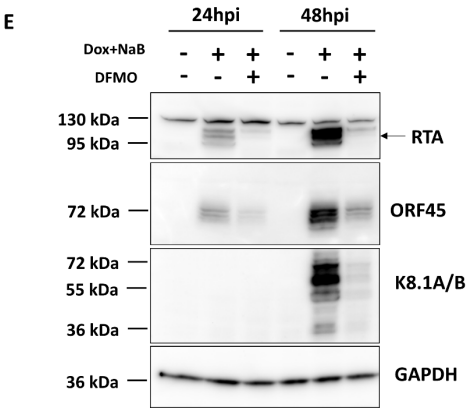
24hpi
48hpi
Dox+NaB
DFMO
130 kDa
95 kDa
RTA
72 kDa
ORF45
72 kDa
55 kDa
36 kDa
K8.1A/B
36 kDa
GAPDH

F

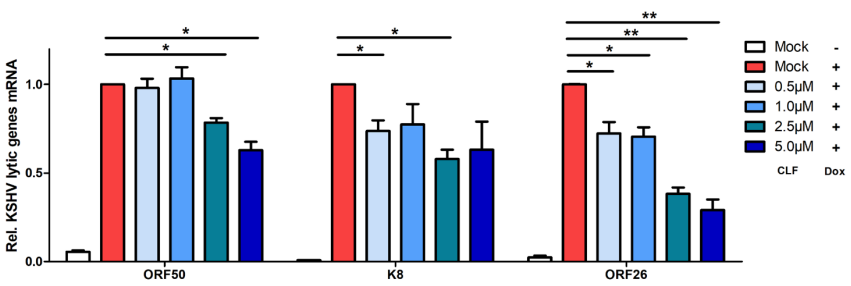
Rel. KSHV lytic genes mRNA
ORF50
K8
ORF26
Mock
Mock
0.5μM
1.0μM
2.5μM
5.0μM
CLF
Dox

865 **Figure 4. Polyamine depletion efficiently blocks KSHV lytic reactivation.** (A, B).
866 HEK293.r219 cells pretreated with progressively increasing doses of 2-difluoromethylornithine
867 (DFMO) for 24h were subsequently induced by ectopic expression of ORF50 for 48h or left
868 un-induced using the empty vector. Above cells were then visualized by fluorescence imaging
869 (A). mRNA level of KSHV K8/K-bZIP (left panel) and latent genes (ORF71/v-FLIP, ORF72/v-
870 Cyclin, and ORF73/LANA; right panel) in above cells were analyzed by RT-qPCR assays and
871 normalized to mock-treated induced cells. The drug effect at a series of doses was plotted as
872 percentage of maximum response by using GraphPad PRISM 5. Relative copy number of
873 KSHV genomes (middle panel) was also analyzed. IC_{50} was determined for DFMO's inhibitory
874 effect. (C). Exogenous polyamines (mixed polyamines supplement [PA Supp, 5x], Spermidine
875 [Spd, 10μM] or Spermine [Spm, 10μM]) were complemented into the culture media of
876 HEK293.r219 cells treated with DFMO (500μM) and induced by ectopic expression of ORF50
877 for 48h or left un-induced using the empty vector. The above cells were labelled with Hoechst
878 and visualized by fluorescence imaging to determine percentage of RFP-positive cells (left
879 panel). mRNA level of KSHV lytic genes (K8/K-bZIP [middle panel], ORF26 [right panel]) in
880 above cells were analyzed by RT-qPCR assays. All results were normalized to mock-treated
881 ORF50-induced cells. (D, E). mRNA level of KSHV lytic genes (ORF50/RTA, K8/K-bZIP and
882 ORF26) in iSLK.BAC16 cells pre-treated with increasing doses of DFMO for 24h and
883 subsequently induced by Dox (1μg/mL) + NaB (1mM) for 48h were analyzed by RT-qPCR
884 assays and normalized to mock-treated induced cells (D, left panel). Relative copy number of
885 KSHV genomes in above cells was also analyzed (D, right panel). Protein level of KSHV lytic
886 genes (ORF45, K8.1A/B) was analyzed by immunoblotting (E). GAPDH was used as the
887 loading control. (F). mRNA level of KSHV lytic genes (ORF50/RTA, K8/K-bZIP and ORF26)
888 in iSLK.BAC16 cells pre-treated with increasing doses of clofazimine (CLF) for 24h and
889 subsequently induced by Dox (1μg/mL) for 48h were analyzed by RT-qPCR assays and

890 normalized to mock-treated induced cells. Results were calculated from n=3 independent
891 experiments and presented as mean ± SEM (* $p<0.05$; ** $p<0.01$; *** $p<0.001$, two-tailed
892 paired Student t-test).
893

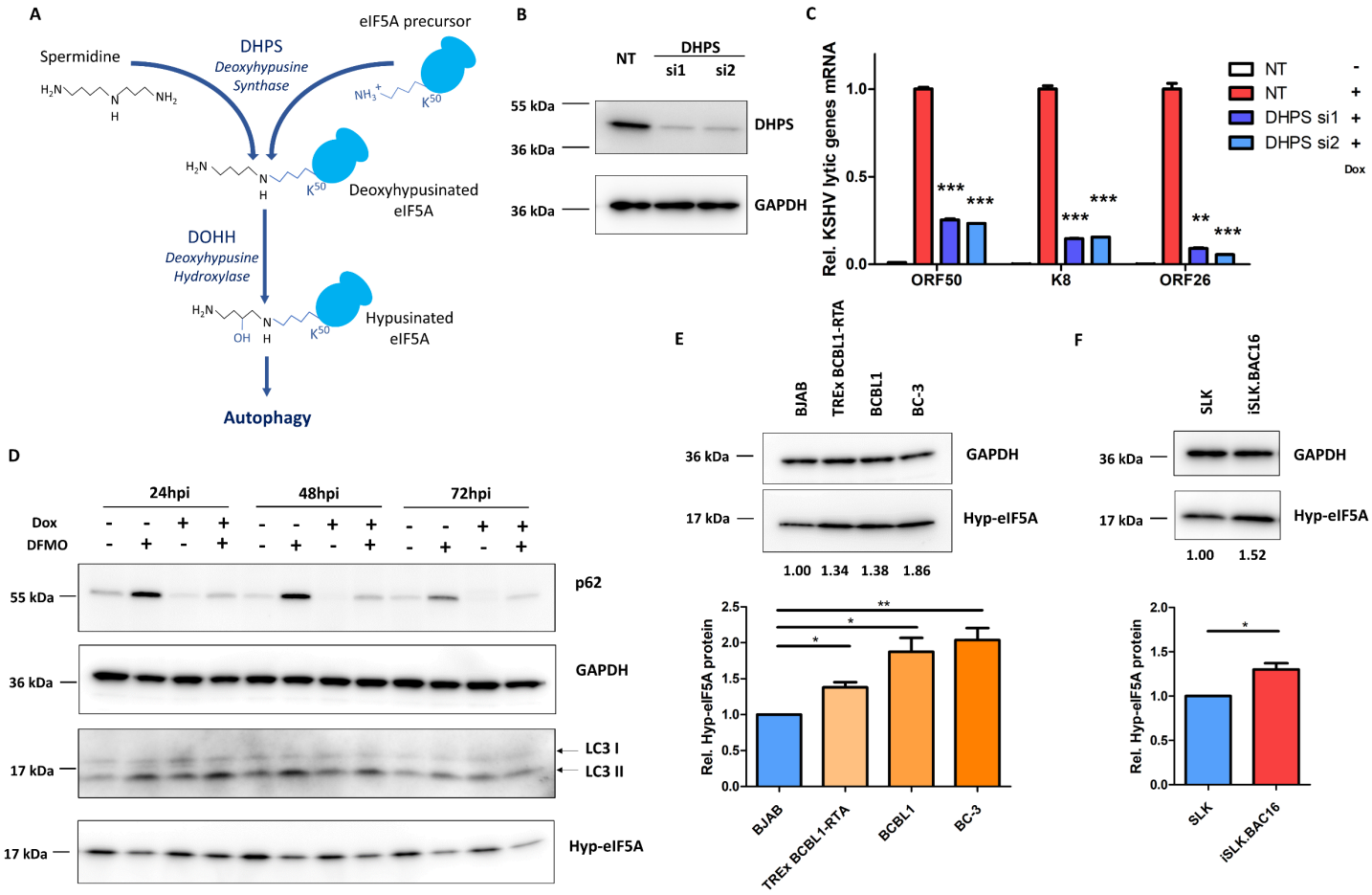

Figure 5. KSHV lytic reactivation depends on eIF5A hypusination. (A). Schematic view of eIF5A hypusination that links spermidine with autophagy activation. (B, C). DHPS knockdown of iSLK.BAC16 cells transfected with DHPS siRNAs (si1, si2) or NT was analyzed by immunoblotting (B). GAPDH was used as a loading control. mRNA level of KSHV lytic genes (ORF50/RTA, K8/K-bZIP and ORF26) in above cells induced with Dox (1μg/mL) was analyzed by RT-qPCR assays and normalized to NT-transfected induced cells (C). (D). Protein level of autophagy markers (p62/SQSTM1, LC3 I/II) as well as hypusine-eIF5A (hyp-eIF5A) in iSLK.BAC16 cells pre-treated with DFMO (500μM) for 24 h and subsequently induced with Dox (1μg/mL) up to 72h was analyzed by immunoblotting assays. GAPDH was used as the loading control. (E, F). Protein level of hyp-eIF5A protein levels in KSHV-infected PEL cells lines (BCBL1 [wild-type], TREx BCBL1-RTA, BC-3) and the KSHV-negative B cell line

906 BJAB (E), or iSLK.BAC16 and SLK cells (F), was analyzed by immunoblotting assays.
907 Intensity of protein bands was determined by using AlphaView SA (software) and normalized
908 to GAPDH. Results were calculated from n=3-4 independent experiments and presented as
909 mean ± SEM (* $p<0.05$; ** $p<0.01$; *** $p<0.001$, two-tailed paired Student t-test).
910

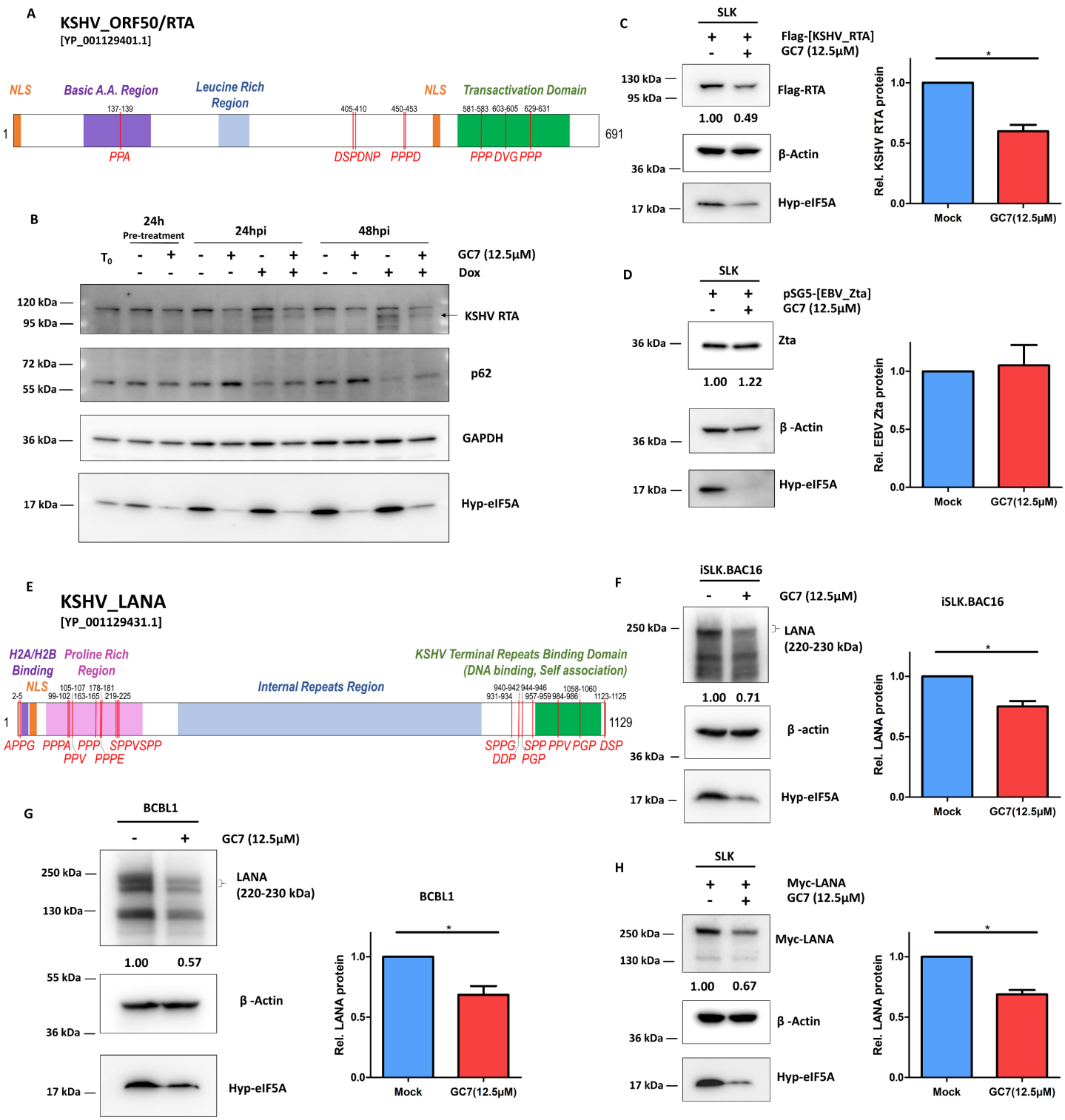

911

912 **Figure 6. Translation of KSHV ORF50/RTA and LANA proteins requires eIF5A**

913 **hypusination.** (A). Schematic view of KSHV ORF50/RTA [YP_001129401.1] with hyp-

914 eIF5A-dependent pause motifs annotated in red and several of its key domains. (B). Protein

915 level of KSHV RTA, p62, and hyp-eIF5A in iSLK.BAC16 cells pre-treated with GC7 (12.5μM)
916 for 24h and subsequently induced with Dox (1μg/mL) up to 48h was analyzed by
917 immunoblotting assays. GAPDH was used as the loading control. (C, D). Protein level of KSHV
918 RTA (C) or EBV Zta (D) along with hyp-eIF5A in SLK cells transfected respectively with the
919 pcDNA vector expressing Flag-tagged KSHV RTA or non-tagged EBV Zta and subsequently
920 treated with GC7 (12.5μM) for 48h was analyzed by immunoblotting assays. β-actin was used
921 as the loading control. (E). Schematic view of KSHV ORF73/LANA [YP_001129431.1] with
922 hyp-eIF5A-dependent pause motifs annotated in red and several of its key domains. (F, G).
923 Protein level of KSHV LANA along with hyp-eIF5A in iSLK.BAC16 (F) or BCBL1 (G) cells
924 treated with GC7 (12.5μM) for 48h was analyzed by immunoblotting assays. β-actin was used
925 as the loading control. (H). Protein level of KSHV LANA along with hyp-eIF5A in SLK cells
926 transfected with the pcDNA vector expressing myc-tagged KSHV LANA and subsequently
927 treated with GC7 (12.5μM) for 48h was analyzed by immunoblotting assays. β-actin was used
928 as a loading control. Intensity of KSHV protein bands was determined by using AlphaView SA
929 (software) and normalized to β-actin. Results were calculated from on n=2-3 independent
930 experiments and presented as mean ± SEM (* $p<0.05$; ** $p<0.01$; *** $p<0.001$, two-tailed
931 paired Student t-test).

932

933

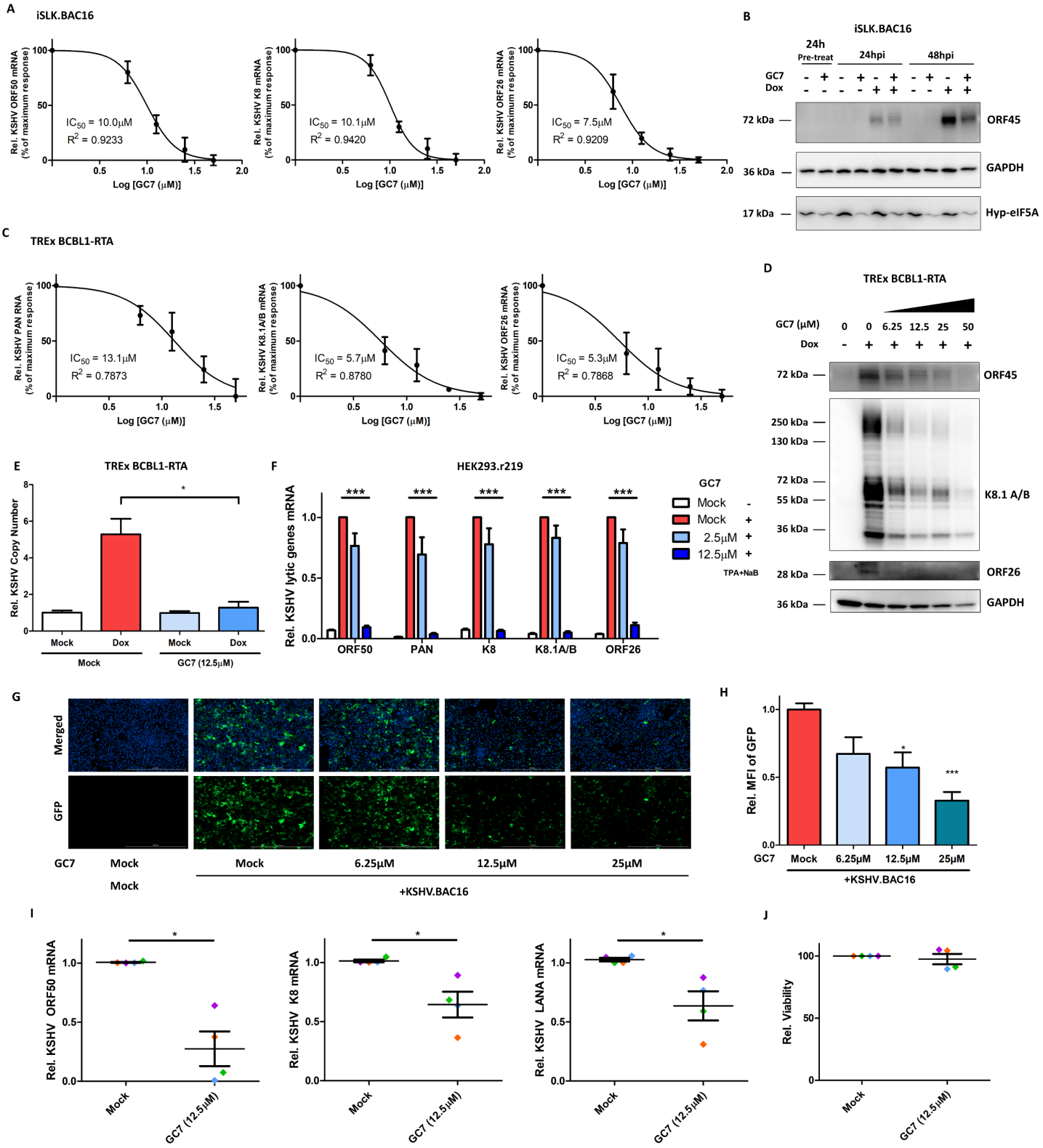

934

935 **Figure 7. Inhibition of eIF5A hypusination efficiently blocks KSHV lytic infection.**

936 (A). mRNA level of KSHV lytic genes (ORF50/RTA, K8/K-bZIP and ORF26) in iSLK.BAC16
937 cells pre-treated with progressively increasing doses of GC7 for 24h and subsequently induced
938 with Dox (1μg/mL) for 48h were analyzed by RT-qPCR assays and normalized to mock-treated
939 induced cells. The drug effect at a series of doses was plotted as percentage of maximum
940 response by using GraphPad PRISM 5. IC_{50} was determined for GC7's inhibitory effect. (B).
941 Protein level of KSHV ORF45 and hyp-eIF5A in iSLK.BAC16 cells pre-treated with GC7
942 (12.5μM) for 24h and subsequently induced with Dox (1μg/mL) up to 48h was analyzed by
943 immunoblotting assays. GAPDH was used as the loading control. (C-E). mRNA level of KSHV
944 lytic genes (PAN RNA, K8.1, ORF26) in TREx BCBL1-RTA cells pre-treated with
945 progressively increasing doses of GC7 for 24h and subsequently induced with Dox (1μg/mL)
946 for 48h were analyzed by RT-qPCR assays and normalized to mock-treated induced cells. The
947 drug effect at a series of doses was plotted as percentage of maximum response by using
948 GraphPad PRISM 5 (C). IC_{50} was determined for GC7's inhibitory effect. Protein level of
949 KSHV lytic genes (ORF45, K8.1A/B, ORF26) in above cells was analyzed by immunoblotting
950 assays (D). GAPDH was used as the loading control. Relative copy number of KSHV viral
951 genomes was also determined (E). (F). mRNA level of KSHV lytic genes (ORF50/RTA, PAN,
952 K8, K8/K-bZIP, ORF26) in HEK293.r219 cells pre-treated with GC7 for 24h and subsequently
953 induced with TPA (20 ng/mL) + NaB (0.3mM) for 48h was analyzed by RT-qPCR assays and
954 normalized to mock-treated induced cells. (G, H). SLK cells were *de novo* infected with KSHV
955 BAC16 viruses (MOI=0.5). Unbound viruses were washed away, and cells were subsequently
956 treated with increasing doses of GC7 for 48h, then subjected to fluorescence imaging analysis
957 (G). Nuclei were labelled with Hoechst (Blue), while GFP expression indicated infection with
958 KSHV BAC16 viruses. MFI of GFP expression from five different fields of view for ≥7000
959 cells was measured and normalized to mock-treated cells (H). (I, J). Primary tonsillar B cells
960 isolated from 4 healthy donors were *de novo* infected with KSHV BAC16 viruses (MOI=3).

961 Unbound viruses were washed away, and cells were subsequently treated with GC7 (12.5 μM)
962 for 72h, followed by RT-qPCR assays to measure mRNA level of KSHV lytic genes
963 (ORF50/RTA, K8/K-bZIP) and latent gene (ORF73/LANA) and normalized to mock-treated
964 cells (I). Cell viability was analyzed by CellTiter-Glo assays and normalized to mock-treated
965 cells (J). Results were calculated from n=3 independent experiments and presented as mean ±
966 SEM (* $p<0.05$; ** $p<0.01$; *** $p<0.001$, two-tailed paired Student t-test).
967

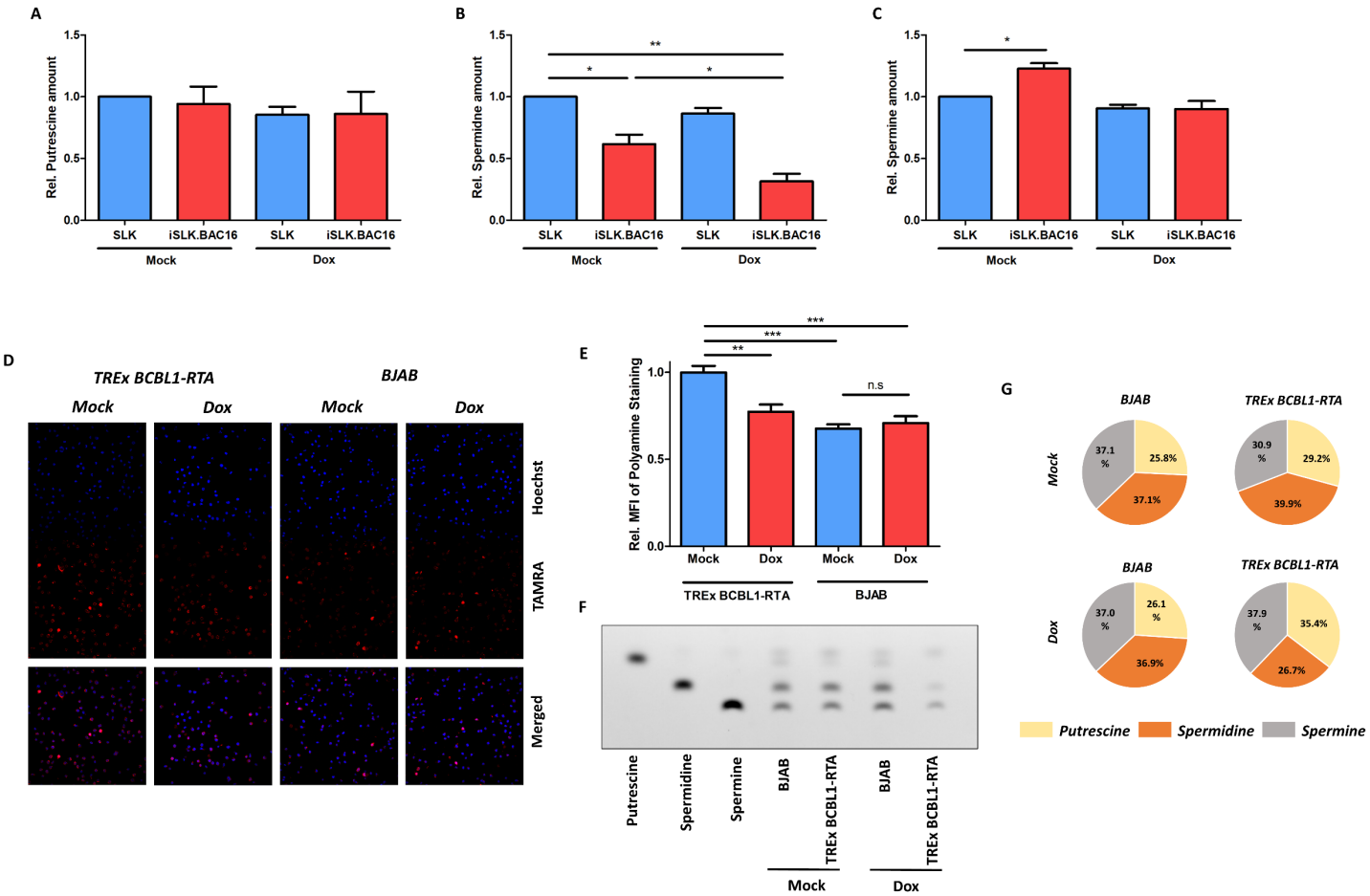

968

969 **Figure S1.** (A-C). Relative abundance of putrescine (A), spermidine (B), and spermine (C)
970 in Figure 1C. (D, E). Intracellular polyamines in TREx BCBL1-RTA and BJAB cells treated
971 with Dox for 48h or mock were stained with PolyamineRED (TAMRA) and visualized by
972 confocal fluorescence microscopy (D), whereas nuclei were labelled with Hoechst (Blue).
973 Mean fluorescence intensity (MFI) of polyamine fluorescence signal (TAMRA) of ≥ 2400 cells
974 (E) was determined and normalized to mock-treated TREx BCBL1-RTA cells. (F, G).
975 Intracellular polyamine species (putrescine, spermidine, spermine) in TREx BCBL1-RTA and
976 BJAB cells treated with Dox for 48h or mock were analyzed by thin-layer chromatography
977 (TLC) with pure individual polyamine species as reference (F). Relative changes of polyamine
978 species in TLC results were displayed as the relative proportion of total intracellular polyamines

979 in pie chart (G). Results were calculated from n=2-3 independent experiments and presented as

980 mean ± SEM (* $p<0.05$; ** $p<0.01$; two-tailed paired Student t-test).

981

982

983

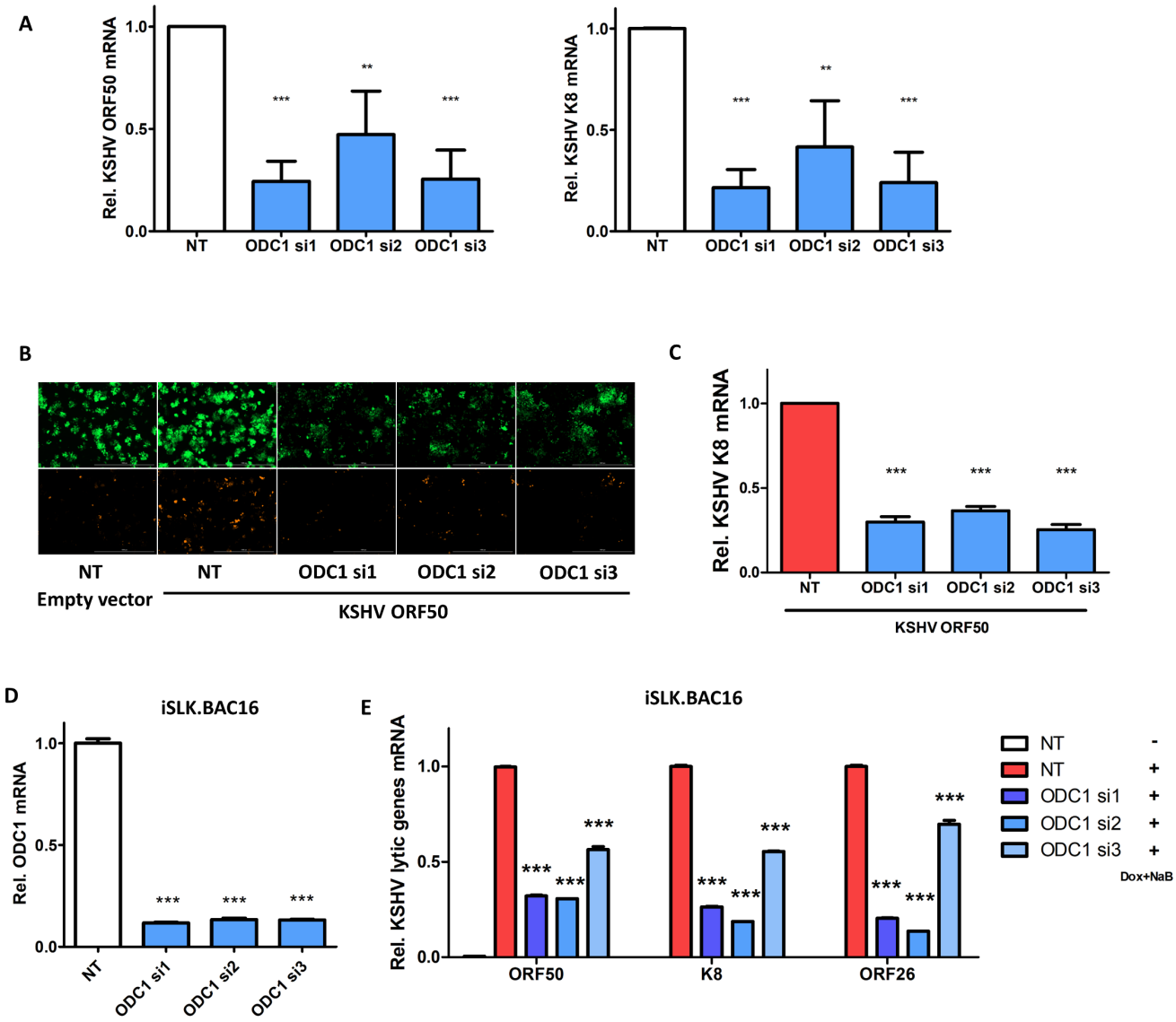

Figure S2. (A). mRNA level of KSHV lytic genes (ORF50/RTA, K8) in un-induced HEK293.r219 cells transfected with ODC1 siRNAs (si1, si2, si3) or non-targeting control siRNA (NT) was analyzed by RT-qPCR assays and normalized to NT-transfected cells. (B, C). HEK293.r219 cells transfected with ODC1 siRNAs (si1, si2, si3) or NT were induced with ectopic expression of ORF50 for 48h and visualized by fluorescence imaging (B). mRNA level of KSHV lytic gene K8 in above cells was analyzed by RT-qPCR assays and normalized to NT-transfected ORF50-induced cells. (D, E). mRNA level of ODC1 (D) and KSHV lytic genes (ORF50/RTA, K8, ORF26; E) in iSLK.BAC16 cells transfected with ODC1 siRNAs (si1, si2, si3) or NT and subsequently induced with Dox (1μg/mL) + NaB (1mM) for 48h was analyzed

994 by RT-qPCR assays and normalized to NT-transfected induced cells. Results were calculated
995 from n=3 independent experiments and presented as mean ± SEM (* $p<0.05$; ** $p<0.01$; ***
996 $p<0.001$; two-tailed paired Student t-test).
997

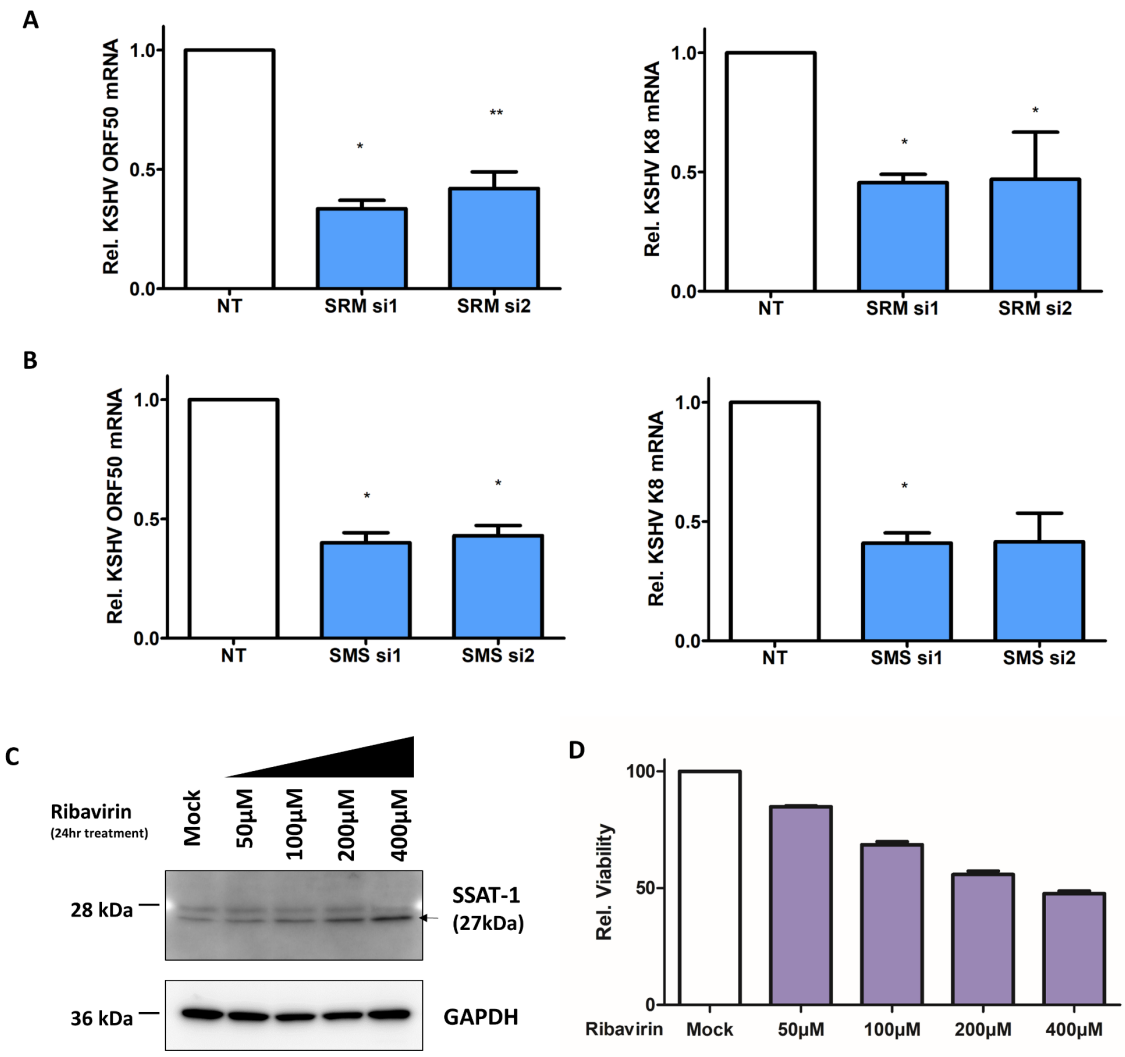

998

999 **Figure S3.** (A, B). mRNA level of KSHV lytic genes (ORF50/RTA, K8) in un-induced
1000 HEK293.r219 cells transfected with siRNAs targeting SRM (si1, si2; A) or SMS (si1, si2; B),
1001 or NT was analyzed by qRT-assays and normalized to NT-transfected cells. (C, D). Protein
1002 level of SSAT-1 in iSLK.BAC16 cells treated with increasing doses of ribavirin for 24h was
1003 analyzed by immunoblotting assays (C). GAPDH was used as the loading control. Cell viability
1004 of above cells was analyzed by CellTiter-Glo assays and normalized to mock-treated cells (D).
1005 Results were calculated from n=2-3 independent experiments and presented as mean ± SEM (*
1006 $p<0.05$; ** $p<0.01$; two-tailed paired Student t-test).

1007

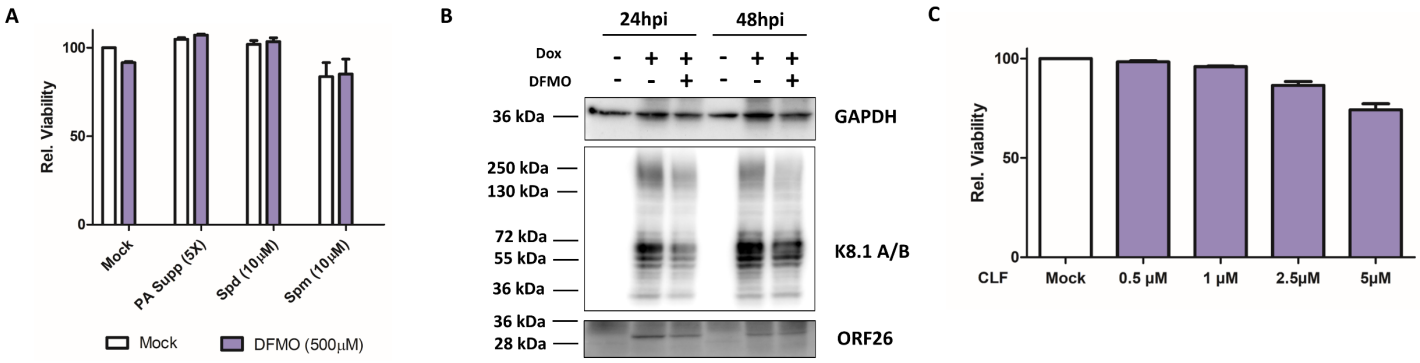

1008

1009 **Figure S4.** (A). Cell viability of HEK293.r219 cells treated with or without exogenous
1010 polyamines (mixed polyamines supplement [PA Supp, 5x], Spermidine [Spd, 10μM] or
1011 Spermine [Spm, 10μM]) in the presence or absence of DFMO (500μM) for 24h was analyzed
1012 by CellTiter-Glo assays and normalized to mock-treated cells. (B). Protein level of KSHV lytic
1013 genes (K8.1A/B, ORF26) in TREx BCBL1-RTA cells pre-treated with DFMO (500μM) for
1014 24h and subsequently induced with Dox (1μg/mL) for 48h was analyzed by immunoblotting
1015 assays. GAPDH was used as the loading control. (C). Cell viability of iSLK.BAC16 cells
1016 treated with increasing doses of clofazimine (CLF) for 24h was analyzed by CellTiter-Glo
1017 assays and normalized to mock-treated cells. Results were calculated from n=3 independent
1018 experiments and presented as mean ± SEM.

1019

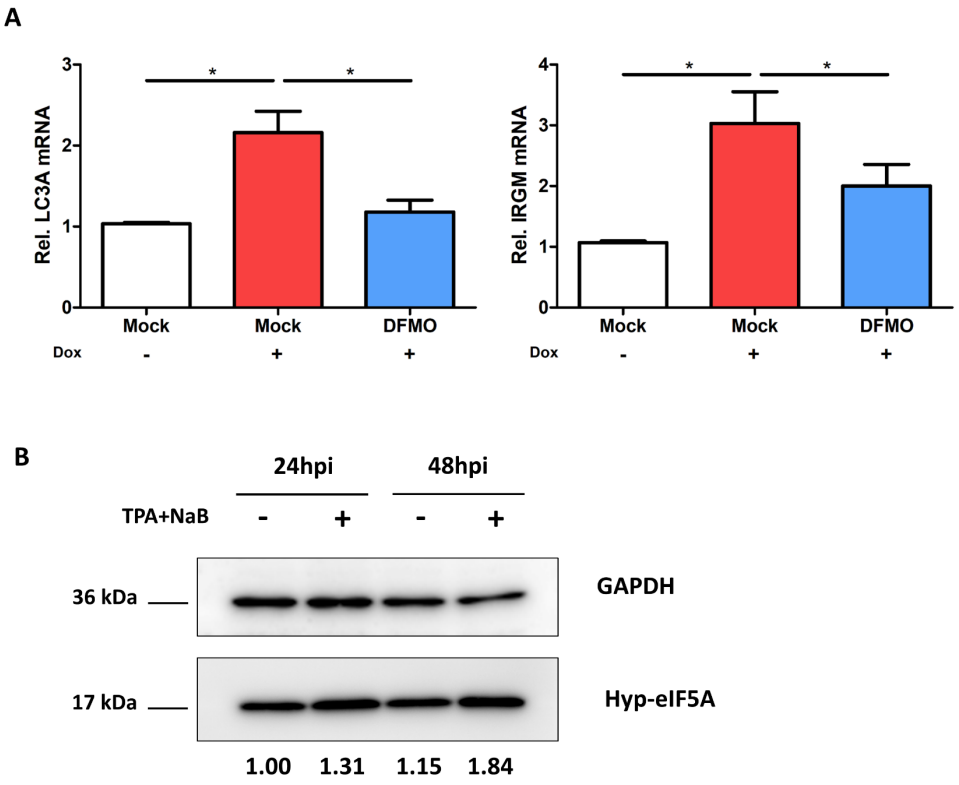

1020

1021 **Figure S5.** (A). mRNA level of autophagy genes (LC3A, IRGM) in iSLK.BAC16 cells pre-
1022 treated with DFMO (500μM) for 24h and subsequently induced with Dox (1μg/mL) for 48h
1023 was analyzed by RT-qPCR assays and normalized to mock-treated un-induced cells. (B).
1024 Protein level of hypusine-eIF5A in HEK293.r219 cells induced with TPA (20ng/mL) + NaB
1025 (0.3mM) for 48h was analyzed by immunoblotting assays. GAPDH was used as the loading
1026 control. Results were calculated from n=3 independent experiments and presented as mean ±
1027 SEM (* $p<0.05$, two-tailed paired Student t-test).

1028

1029

A

GPP	DPP	PPP	SPP	PPG	PPA	PPV	PPE
PPD	APP	MPP	DSP	DDP	PDP	DNP	DGP
PDK	PDG	GDP	PDI	PGP	PDR	DPG	RDK
PDA	PDV	DVG	DDG	GGT			

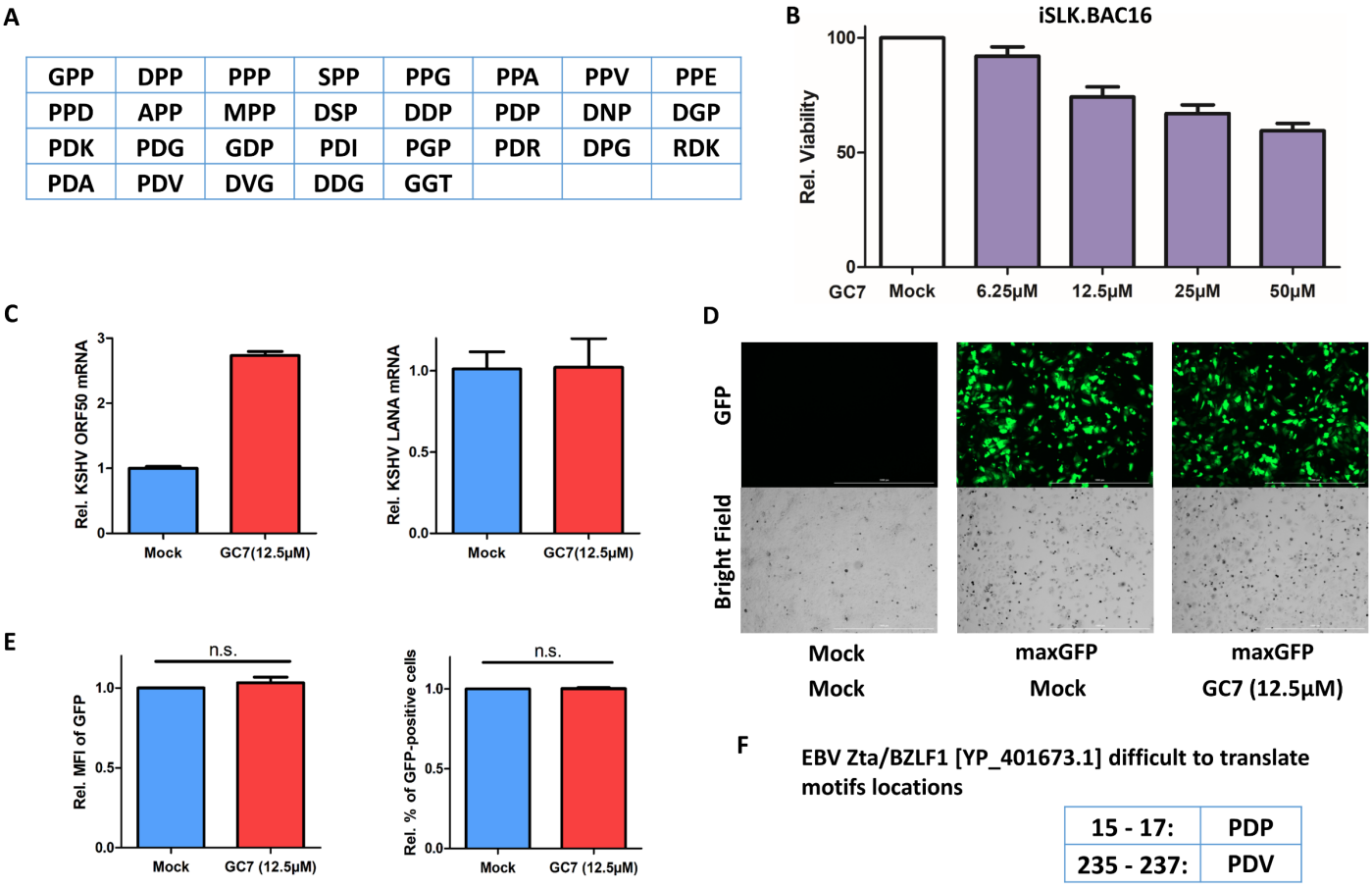

F

EBV Zta/BZLF1 [YP_401673.1] difficult to translate motifs locations

15 - 17:	PDP
235 - 237:	PDV

Figure S6. (A). List of hyp-eIF5A-dependent pause motifs reported in Schuller et al. 2017 [17]. (B). Cell viability of iSLK.BAC16 cells treated with increasing doses of GC7 for 24h was analyzed by CellTiter-Glo assays and normalized to mock-treated cells. (C). mRNA level of transfected KSHV ORF50/RTA or ORF73/LANA cDNA in GC7-treated SLK cells was analyzed by RT-qPCR assays and normalized to mock-treated cells. (D, E). SLK cells transfected with pmaxGFP (Lonza) and subsequently treated with GC7 (12.5μM) were visualized by fluorescence imaging (D). These cells were also analyzed by flow cytometry, and relative MFI of GFP expression as well as percentage of GFP-positive cells was determined (E). (F). List of hyp-eIF5A-dependent pause motifs in the coding sequence of EBV Zta protein (YP_401673.1). Results were calculated from n=3 independent experiments and presented as mean ± SEM (ns: not significant, two-tailed paired Student t-test).

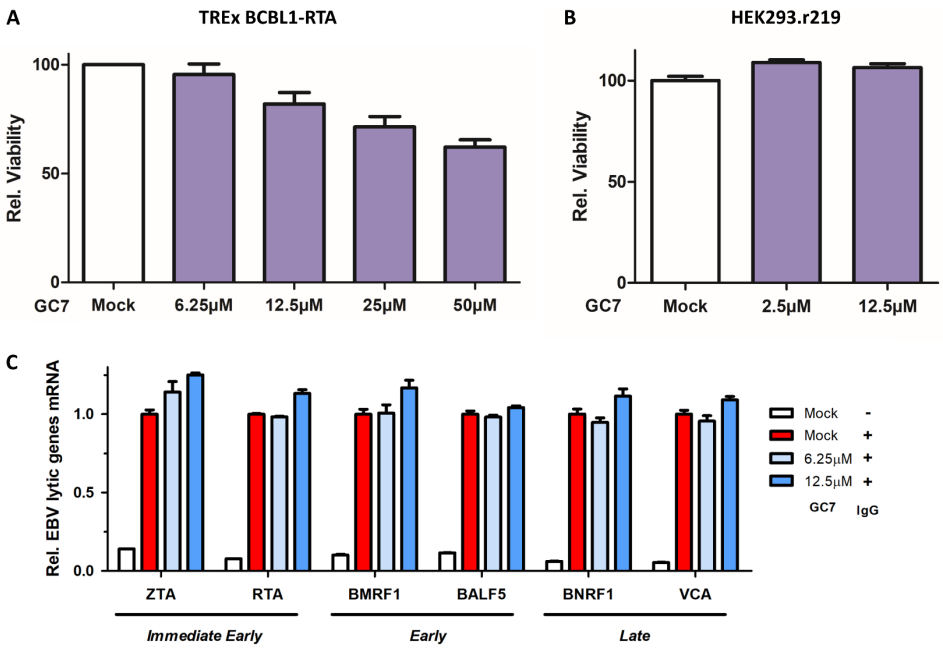

1042

1043 **Figure S7.** (A, B). Cell viability of TREx BCBL1-RTA (A) and HEK293.r219 (B) cells
1044 treated with increasing doses of GC7 for 24h was analyzed by CellTiter-Glo assays and
1045 normalized to mock-treated cells. (C) mRNA level of indicated EBV lytic genes in Akata/BX
1046 cells pre-treated with GC7 for 24h and subsequently induced with human IgG for 48h was
1047 analyzed by RT-qPCR assays and normalized to mock-treated IgG-induced cells. Results were
1048 calculated from n=2-3 independent experiments and presented as mean ± SEM.

1049

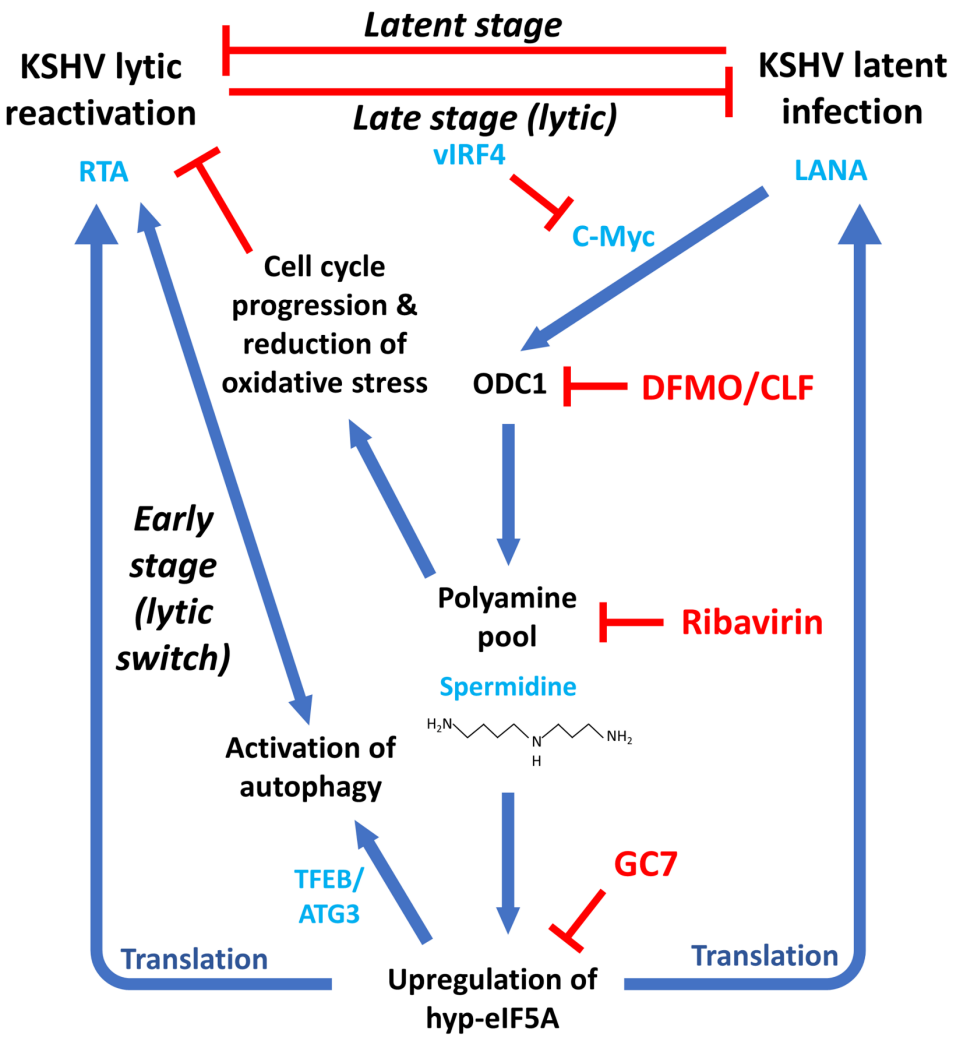

1050

1051 **Figure S8. A proposed model illustrates the dynamic and profound interaction of host**
1052 **polyamine biosynthesis and eIF5A hypusination with KSHV infection.** At the stage of latent
1053 infection, KSHV ORF73/LANA protein induces upregulation of c-Myc that further
1054 transcriptionally activates ODC1, which results in the overall increase of intracellular
1055 polyamines. However, spermidine is consumed to produce hypusine-eIF5A ensuring the
1056 efficient translation of LANA protein required for maintenance of KSHV latency. This results
1057 in a positive feedback sustaining activation of the polyamine-hypusine axis. At the early stage
1058 of lytic switch, KSHV ORF50/RTA gene starts to be actively transcribed upon certain stimuli,
1059 and the constant high level of hypusine-eIF5A not only ensures the efficient translation of RTA
1060 protein but also facilitates the activation of autophagy, which overall promotes KSHV lytic

1061 reactivation. On the contrary, at the late stage of lytic replication KSHV RTA protein is
1062 expressed up to a sufficient level to suppress LANA protein, leading to decrease of ODC1 and
1063 reduction of intracellular polyamines. In addition, other KSHV lytic proteins, such as vIRF4,
1064 also contribute to the downregulation of c-Myc, causing further decrease of ODC1 and
1065 polyamines. This would generate an adverse effect on cell cycle progression and an increase of
1066 oxidative stress, which would be beneficial to KSHV lytic reactivation. Thus, cells are now
1067 adjusted to a favorable environment to further promote KSHV lytic replication and viral
1068 propagation. KSHV *de novo* infection likely suppresses ODC1 as well to allow early steps of
1069 viral replication. Given to the critical roles of polyamine biosynthesis and eIF5A hypusination
1070 in KSHV infection, inhibitors targeting these metabolic pathways would serve as novel antiviral
1071 reagents to efficiently block both KSHV latent and lytic replications.

1072

1073

Table S1. List of hyp-eIF5A-dependent pause motifs in the coding sequence of ORF50/RTA protein from multiple KSHV strains.

Human herpesvirus 8 type M, partial genome
GenBank: U75698.1

ORF 50 [Human herpesvirus 8 type M] GenBank: AAC57132.1
631 aa

Amino Acid position	Tri-Peptide motif
Pattern: **PPA**	
77 - 79:	PPA
Pattern: **DSP**	
345 - 347:	DSP
Pattern: **DNP**	
348 - 350:	DNP
Pattern: **PPP**	
390 - 392:	PPP
521 - 523:	PPP
569 - 571:	PPP
Pattern: **PPD**	
391 - 393:	PPD
Pattern: **DVG**	
543 - 545:	DVG

Human herpesvirus 8 strain KSHV-BAC36 long unique region, genomic sequence
GenBank: HQ404500.1

ORF50 protein [Human gammaherpesvirus 8] GenBank: ADQ57929.1
691 aa

Amino Acid position	Tri-Peptide motif
Pattern: **PPA**	
137 - 139:	PPA
Pattern: **DSP**	
405 - 407:	DSP
Pattern: **DNP**	
408 - 410:	DNP
Pattern: **PPP**	
450 - 452:	PPP
581 - 583:	PPP
629 - 631:	PPP
Pattern: **PPD**	
451 - 453:	PPD
Pattern: **DVG**	
603 - 605:	DVG

Human herpesvirus 8 strain JSC-1 clone BAC16, complete genome [GenBank: GQ994935.1]

ORF50 [Human gammaherpesvirus 8] GenBank: ACY00448.1
691 aa

Amino Acid position	Tri-Peptide motif
Pattern: **PPA**	
137 - 139:	PPA
Pattern: **DSP**	
405 - 407:	DSP
Pattern: **DNP**	
408 - 410:	DNP
Pattern: **PPP**	
450 - 452:	PPP
581 - 583:	PPP
629 - 631:	PPP
Pattern: **PPD**	
451 - 453:	PPD
Pattern: **DVG**	
603 - 605:	DVG

Table S2. List of hyp-eIF5A-dependent pause motifs in the coding sequence of ORF73/LANA protein from multiple KSHV strains.

Human herpesvirus 8 type M, partial genome
GenBank: U75698.1

ORF 73 [Human herpesvirus 8 type M] GenBank: AAC57158.1 – 1162 aa / 19 HITS
1162 aa

Amino Acid position	Tri-Peptide motif
Pattern: **APP**	
2 - 4:	APP
Pattern: **PPG**	
3 - 5:	PPG
965 - 967:	PPG
Pattern: **PPP**	
99 - 101:	PPP
163 - 165:	PPP
178 - 180:	PPP
Pattern: **PPA**	
100 - 102:	PPA
USERPAT7 :	
Pattern: **PPV**	
105 - 107:	PPV
220 - 222:	PPV
1017 - 1019:	PPV
Pattern: **PPE**	
179 - 181:	PPE
Pattern: **SPP**	
219 - 221:	SPP
223 - 225:	SPP
964 - 966:	SPP
990 - 992:	SPP
Pattern: **DDP**	
973 - 975:	DDP
Pattern: **PGP**	
977 - 979:	PGP
1091 - 1093:	PGP
Pattern: **DSP**	
1156 - 1158:	DSP

Human herpesvirus 8 strain KSHV-BAC36 long unique region, genomic sequence GenBank: HQ404500.1

LANA [Human gammaherpesvirus 8] GenBank: ADQ57959.1- 1117 aa / 17HITS 1117 aa

Amino Acid position	Tri-Peptide motif
Pattern: **APP**	
2 - 4:	APP
Pattern: **PPG**	
3 - 5:	PPG
920 - 922:	PPG
Pattern: **PPP**	
99 - 101:	PPP
163 - 165:	PPP
178 - 180:	PPP
Pattern: **PPA**	
100 - 102:	PPA
Pattern: **PPE**	
179 - 181:	PPE
Pattern: **SPP**	
219 - 221:	SPP
223 - 225:	SPP
919 - 921:	SPP
945 - 947:	SPP
Pattern: **PPV**	
220 - 222:	PPV
972 - 974:	PPV
Pattern: **DDP**	
928 - 930:	DDP
Pattern: **PGP**	
932 - 934:	PGP
Pattern: **DSP**	
1111 - 1113:	DSP

Human herpesvirus 8 strain JSC-1 clone BAC16, complete genome [GenBank: GQ994935.1]

ORF73 [Human gammaherpesvirus 8] GenBank: ACY00477.1 – 1123 aa /19 HITS 1123 aa

Amino Acid position	Tri-Peptide motif
Pattern: **APP**	
2 - 4:	APP
Pattern: **PPG**	
3 - 5:	PPG
926 - 928:	PPG
Pattern: **PPP**	
99 - 101:	PPP
163 - 165:	PPP
178 - 180:	PPP
Pattern: **PPA**	
100 - 102:	PPA
Pattern: **PPV**	
105 - 107:	PPV
220 - 222:	PPV
978 - 980:	PPV
Pattern: **PPE**	
179 - 181:	PPE
Pattern: **SPP**	
219 - 221:	SPP
223 - 225:	SPP
925 - 927:	SPP
951 - 953:	SPP
Pattern: **DDP**	
934 - 936:	DDP
Pattern: **PGP**	
938 - 940:	PGP
1052 - 1054:	PGP
Pattern: **DSP**	
1117 - 1119:	DSP

Table S3. List of PCR primers used in this study

Gene	Forward (5' to 3')	Reverse (5' to 3')
KSHV_ORF50	CCTTCGGCCCGGGGTCT	CGGTGGCAGTTGCGTATACTCT
KSHV_K8	CCTGGACGCTCTCTCACACA	GGATCTGCGAGTTGGAAGCT
KSHV_PAN	ATAGGCGACAAAGTGAGGTGGCAT	TAACATTGAAAGAGCGCTCCCAGC
KSHV_K8.1A/B	AAAGCGTCCAGGCCACCACAGA	GGCAGAAAATGGCACACGGTTAC
KSHV_ORF26	AGCCGAAAGGATTCCACCAT	TCCGTGTTGTCTACGTCCAG
KSHV_LANA	TTACCTCCACCGGCACTCTT	GGATGGGATGGAGGGATTG
GAPDH	GCCTCTTGTCTCTTAGATTTGGTC	TAGCACTCACCATGTAGTTGAGGT
ODC1	TGCTGCTGCCTCTACGTTCA	CCACGCAGGCCCTGAC
AGMAT	TGGGAGGCAAACCCATTTAT	CTAGGAGTGAGACCAGCAATTT
SRM	CTACATGTGGGTGACGGTTT	GACTCCTTGAAGAGACTTTCGG
SMS	GATCGTCTGTGTCCCTTCATAC	GGCTACTGATCTTCAGGGTTTAG
LC3A	CGCTACAAGGGTGAGAAGCA	AGAAGCCGAAGGTTTCCTGG
IRGM	GCAGATGGGAACTTGCCAGA	AGGCCTTACCCTCATGTCCT
EBV_BZLF1	AATGCCGGGCCAAGTTTAAGCAAC	TTGGGCACATCTGCTTCAACAGGA
EBV_BRLF1	TGGCTTGGAAGACTTTCTGAGGCT	AATCTCCACACTCCCGGCTGTAAA
EBV_BMRF1	ATACGGTCAGTCCATCTCCT	CACTTTCTTGGGGTGCTT
EBV_BALF5	GCGGCCCCGGAGTTGTTA	CGTGGCCGTGGATCATTATTTC
EBV_BNRF1	GCAAACATACAGGAGGAAAG	CAGCAGGTTCTCAGCAATC
EBV_BLLF1	GCCTTGGAGAATATAACCTTG	CATTACTGTCTCGGGTCTTGG
EBV_BcLF1	GTGGATCAGGCCGTTATTGA	CCTCAAACCCGTGGATCATA

1074